Indo-Pacific oceanic connection and ENSO events observed and simulated with a Pacific ocean-atmosphere model forced over 1980-1998

by

Pierre Florenchie and Claire Perigaud(*)

Submitted to Climate Dynamics

March 10th, 2000.

Address: Jet Propulsion Laboratory, California Institute of Technology, MS 300/323, 4800 Oak Grove Dr., Pasadena, CA 91109, USA.

(*) To whom correspondence should be addressed:
Phone= 818 354 8203, fax= 818 393 6720, email=cp@pacific.jpl.nasa.gov

Abstract. In situ and satellite sea level data sets over 1980-1998 are used to estimate the interannual variations of the geostrophic zonal transport across the opening of the Northwestern Pacific boundary into the Celebes sea. This transport agrees with available estimates of the Indonesian ThroughFlow. It tends to increase to the West during La Niña events. It is also consistent with the transport estimated between Java and Australia when adding the waters coming from the South Indian ocean. It can be used, after removing the transport component due to the Pacific wind-driven and fully-reflected equatorial waves, to correct for the closed boundary of the model. This correction, named ITF, varies by a few Sverdrups. Its inflows/outflows are leading the warm/cold events by a few months. The ITF variations are then prescribed at the western boundary during a model integration over 1980-1998 to compare with the simulations obtained with a closed boundary. An ITF inflow anomaly makes the SST slightly warmer in the eastern Pacific and the trade winds slightly weaker in the central Pacific. Indeed these quantities are simulated by both model experiments in very good agreement with the observations. More importantly, prescribing the ITF variations affects quantities that are essential for the coupled simulations. Thus, it improves the sea level variability along the equator by shifting to the west the position of the minimum amplitude closer to the dateline. Also in better agreement with observations, it amplifies the basin-averaged changes of the equatorial Pacific sea level and introduces an interdecadal trend South of the equator that is absent in the experiment with closed boundary.

I - Introduction

Most of the coupled models used to study the El Nino Southern Oscillations (ENSO) rely on a tropical Pacific ocean model with closed boundaries. In reality, the western boundary of the Pacific ocean is not closed. The Indonesian Throughflow connects dynamically and thermodynamically the Indian and the Pacific oceans (Gordon, 1986; Godfrey, 1996; Schneider, 1998). Its mean transport contributes to warm up the eastern Indian ocean and cool down the western Pacific warm pool. Its variations are expected to be involved in those of the coupled ocean-atmosphere system, including remote areas such as the cold tongue, but little is known today about how the coupled mechanisms actually work. Indeed a lot is unknown about the Indonesian Throughflow transport itself. Wyrtki (1987) estimated the Throughflow variations by taking the sea level differences between Davao in the western Pacific and Darwin in the eastern Indian ocean and found that they were linked to the ENSO. Further observations (Meyers, 1996; Fieux et al, 1996) and model simulations (Kindle et al, 1989; Clarke and Liu, 1994; Vershell et al., 1995; Murtugudde et al., 1998) support that there is such a relationship. The transport from the Pacific to the Indian ocean tends to be weaker during El Niño and stronger during La Niña. As warm and cold events are well correlated with equatorial westerlies and easterlies in the central Pacific, the Throughflow interannual variability is explained to a large extent by the equatorial Pacific winds (Murtugudde et al., 1998). But the various published transport estimates differ by several Sverdrups from each other. In addition, the correlation between the transport variations and ENSO is not high and other factors than ENSO in the equatorial

Pacific probably affect the transport. The Throughflow corresponds to the pressure exerted by the entire Pacific onto the Indian ocean and it involves off-equatorial processes as well. The mean Throughflow transport and its low-frequency variations are expected to be in balance with the wind curl over the Pacific basin (or the Indian/Atlantic oceans) as far as 45°S South of Tasmania (Godfrey, 1989; Wajsowicz, 1995; Godfrey, 1996). Because of incomplete data sets, inaccuracies and differences in model assumptions, the various estimates published in the literature bear a large uncertainty.

The purpose of our study is to investigate the impact of the Indo-Pacific connection on ENSO. For this, we use a model of the tropical Pacific ocean coupled to a statistical atmosphere and carry on experiments with various conditions applied at the western boundary. This coupled model can be integrated in time either in a "forced" or a "coupled" context. This paper is devoted to experiments in the "forced" context. It means that the observed wind stress anomalies force the ocean model which delivers the simulated sea level and sea surface temperature (SST) anomalies, the latter being used to force the atmosphere which finally delivers the simulated wind stress anomalies. In the "coupled" context, the wind is estimated at each time step by the statistical atmosphere using the simulated SST, and the model is integrated in time without data insertion. Because the understanding of the coupled mechanisms is still very premature in comparison of how the wind-driven ocean works, results on the coupled mechanisms are reported elsewhere (paper to be submitted).

An important part of the present paper is the estimate of the transport across the section at 130°E where the Pacific ocean opens to the Banda seas. Because this is not a common procedure for estimating the Throughflow transport variations, we compare our estimate with others that are either available in the literature or determined otherwise, including geostrophic computations across sections in the Southeastern Indian Ocean. But this validation is not the only objective of our paper. Our aim is to correct the model for the fact that it verifies closed boundary conditions in the West Pacific whereas in reality, the Pacific is connected to the Indian Ocean. Such a correction is obtained by removing to the geostrophic transport derived from sea level data, the transport due to the wind and the full reflection of equatorial waves in the Pacific. We call this difference ITF. This method is appropriate to our modeling tools and data. The ITF is representative of the variations due to the Indo-Pacific oceanic connection, to the extent that data are errorless and that the model errors are due to the inappropriate boundary conditions in the Northwestern Pacific only. Because of potential other error sources, another important part of this paper consists in validating the model outputs obtained in the closed boundary case with various oceanic and atmospheric data, and find out whether prescribing the ITF variations during a model integration improves the anomalies simulated away from the western boundary or not.

This paper is organized as follows. In the next section, we describe the satellite and in situ data used to compute the sea level anomalies over the Indian and Pacific oceans between 1980 and 1998. In section 3, we examine various estimates of the

Indonesian Throughflow variations on the Pacific or the Indian side. In section 4, we present and validate the results of the forced experiment with closed western boundary conditions (the control run). Section 5 is dedicated to the estimate of the ITF correction to be applied to the model closed boundary. In section 6, the ITF correction are applied in a model experiment for comparison with the control run and validation with data. After a summary of results, perspectives for the coupled experiments are proposed in Section 7.

2 – Sea Level Data

Sea level data over the Indian and Pacific oceans are estimated from eXpandable BathyThermograph sondes (XBT) between January 1980 and March 1998 and from TOPEX/Poseidon (TP) satellite between October 1992 and June 1998. The XBT data set are the analyzed temperature fields provided by Dr. Smith from Bureau of Meteorology Research Center (Smith, 1995). Actually, this data set does not provide sea level, we computed the surface dynamic height (hdyn) relative to 400m as a proxy. Both data sets are estimated every month with a 1° x 1° resolution.

Monthly varying climatologies have been computed over January 1980-December 1996 for hdyn, and over January 1993-December 1996 for TP to determine the sea level anomalies (SLA). All the results of this paper, for data and model, are anomalies relative to the January 1980-December 1996. So, we added to TP anomalies the surface defined by the average of hdyn anomalies between January 1993 and December 1996 (Fig. 1a). The East and South Pacific (mostly east of the dateline and down to 10°S) is higher over these years than before 1993. By contrast,

the West and North Pacific (mostly West of the dateline and up to 20°N) is lower. These anomalies have an amplitude of 2 to 4 cm and, based on their homogeneity in space, they cannot be noise. In the Indian ocean, the reference surface has weaker anomalies, with negative values occurring in the eastern Indian warm pool (minimum South off the Java coast), and positive values East of 90°E with a maximum south of the equator in the cold tongue of the Indian Ocean. It is striking that on average over 1993-1996, the ocean heat content is in deficit over the Indo-Pacific warm pool and in excess over the cold tongues of the Pacific and Indian oceans, while it was in the opposite situation by the same amount on average between 1980-1992. This anomaly map reveals possible large-scale interdecadal exchanges between the two oceans. It is reminded that adding the reference surface to TP anomalies before using these data to initialize a forecast model is crucial for the predictions (Perigaud and Dewitte, unpublished manuscript).

TP satellite data provide actual sea level whereas hdyn is only a proxy. In addition, TP data have an accuracy of ~ 1 cm whereas errors of several centimeters are made in hdyn because the variations are relative to a fixed depth and because the salinity interannual variations are not accounted for. So the two signals are not expected to perfectly match each other. Because TP data are accurate and because SLA (that include salinity changes) is the appropriate quantity for validating the model (see next sections), we choose to keep TP data when available and to correct hdyn as follows. For each data set, we computed the RMS variability over 1992-1998. Their ratio at each point (Fig.1b) is used to multiply the hdyn time series so that the two

data sets have the same amplitude during the satellite period. Fig. 1b shows that the ratio is close to 1.0 in the equatorial Pacific ocean between 10°S and 10°N. As anticipated, the ratio reach large values elsewhere, even larger than 2.0 in like in the Indian Ocean. Part of it is due to the fact that a deeper level than 400m is needed in the South to account for the full variability associated with the Indonesian Throughflow (Broecker, 1991). Part of it is due to large salinity changes like in the Bay of Bengal and the Southeastern Indian. In addition to these two error sources, Fig.1b suggests that the lack of in situ measurements in some regions is also a source of error for hdyn. The off-equatorial Pacific and the Indian Oceans are indeed poorly covered by XBT data in comparison with the equatorial Pacific.

The hdyn values over 1980-1998 are then multiplied at each point by this ratio in order to match the amplitude observed by TP. This correction does not warranty that the two data sets agree well. Time series estimated by hdyn and TP in two regions of the Pacific or the Indian ocean are presented in Fig. 2 before and after applying the corrections. Before correction, in the Pacific rms differences are 3cm for signals which have rms amplitudes of 8cm and 9cm. In the Indian Ocean, the initial difference is 5 cm for signals of 4cm and 7cm. The agreement is improved when the corrections are applied (rms differences are respectively 2cm and 3cm). These examples in the Indo-Pacific region are fairly representative of how the hdyn and TP estimates agree elsewhere. Correlations are higher than 0.5 and rms differences are smaller than the observed amplitude everywhere after corrections. In the rest of the paper, the 1980 to 1998 time series correspond to the corrected hdyn between January

1980 and September 1992, and to the corrected TP data between October 1992 and June 1998.

3 – Geostrophic estimates of the Throughflow

Geostrophic zonal current anomalies are derived from SLA following the method described in Delcroix at al. (1994) for matching the equatorial points with the off-equatorial ones. Transports are presented across sections in the western Pacific or in the eastern Indian Oceans and compared to other estimates of the Throughflow found in the literature.

Several authors (i.e., Wyrtki, 1987; Mutugudde et al, 1998; Potemra and Lukas, 1999) found that the Throughflow variations can be monitored by taking the sea level differences between the western Pacific warm pool and the eastern Indian Ocean. Time series of SLA observed close to Davao, east of the Philippines at (125°E, 5°N) and Darwin, North of Australia at (122°E, 12°S) are presented in Fig.3a. Both series undergo interannual anomalies. Their smoothed differences (Darwin – Davao) are presented in Fig.3b. When the difference is positive, one can expect the Pacific to exert less pressure than usual on the Indian ocean and the westward Throughflow to be less intense than usual like in 1980-81, 1986-87, and 1996-97. By contrast, years 1983-84, 1988-89 and end of 1992 are periods with increased flow to the west. The correlation between the Throughflow transport and the ENSO signal is thus positive. It is not high though. It is found close to 0.3 (we come back on this issue in section 5). Here, this sea level difference is rather compared to the geostrophic transport variations derived from the SLA in the western Pacific. The

solid line in Fig. 3b represents the transport across 130°E between 2.5°N and 7.5°N. The position and width of this section are chosen to match the latitudes of the ocean opening to the Celebes sea between Mindanao and Halmahera islands. The longitude is slightly to the east of the actual opening in order to avoid data inaccuracies close to the coast. It is also the section which is retained for correcting the boundary conditions of the model (see explanations in Section 5). It is striking that the two time series of Fig.3b are well correlated (0.66). The new result found here is that one can take the geostrophic transport across the opening of the western Pacific boundary only and find variations that have some similarity with the Throughflow variations estimated from the sea level difference between the western Pacific and the Indian ocean. It is indeed possible that the geostrophic transport variations across the Pacific section are linked to the Throughflow variations as this opening corresponds to the main water pathway of the Indonesian Throughflow (Nof, 1996).

In Fig.3b, the transport values in Sverdrups correspond to assuming an homogeneous upper ocean layer of 150m (this also corresponds to the model assumption, see section 4). The maximal westward anomalies of ~5 Sverdrups in 1983-84 and 1988-89 and the minima of ~3 Sv in 1986/87 and ~5 Sv in 1991 agree well in phase and amplitude with the values across the Indonesian channels simulated by Murtugudde et al (1998). However, the positive anomalies in 1994 miss the westward increase found in the latter and rather resemble the results of their experiment with the Indian Ocean driven by climatological winds. So, let us examine now the Throughflow variations that can be estimated on the Indian side.

XBT hydrographic profiles have been regularly measured along a line from Fremantle or Shark Bay (Western Australia) to South Java and used to estimate Indonesian Throughflow transport variations between May 1983 and November 1994 (Meyers, 1996). The time series of SLA observed close to that XBT line at 8°S, 105°E (South of Java) and at 20°S, 110°E (NW Australia) are presented in Fig. 4a. The Java variations have a larger amplitude, especially in late 1994 and 1997. The latter are well explained by strong easterlies blowing then in the equatorial Indian ocean (paper in preparation). The anomalies of the transport estimated by Meyers (1996) using the XBT vertical temperature profiles are reproduced in Fig.4b and correspond to the solid line referred to as "transXBT". Using the surface dynamic topography relative to 400m along the XBT line (data provided by Dr. Meyers) and assuming that the upper ocean has a constant depth to compute the geostrophic transport from sea level as above, provides transport values that do not agree with transXBT. This is because the upper 400m of the ocean have a mean vertical structure which changes a lot along this section, the thermocline being much shallower at Java than West of Australia. The transport represented by the dotted line in Fig. 4b and referred to as "transhdyn", obtained by applying the surface current over a layer thickening from 150m at Java to 400m at 15°S and below, agree reasonably well with transXBT. Finally, we use the 1980-1998 SLA and compute the geostrophic transport across 105°E between 8°S and 20°S (dashed curve in Fig. 4b referred to as "transSLA"), with the same varying upper layer thickness. All the time series presented in Figure 4 confirm Meyers (1996)'s results. In particular, the transport variability is mostly explained by two modes, one on the Australian side (like in

1987-88-89) which is ENSO-related, and one on the Java side (like in 1994 and 1997) which is related to the zonal wind of the equatorial Indian Ocean.

The Indian transport time series of Fig.4b have some resemblance with the Pacific ones of Fig. 3b, in particular for the minimal values of ~5 Sv in 1984 and 1988-89. It is confirmed on both sides that the Throughflow increases during cold events. However, the time series of the two oceans present discrepancies that are large, too large to be realistic. In 1994 they differ by more than 5 Sverdrups. We are certainly aware that it is not possible to compute accurate estimates of the Throughflow transport using sea level data only. But the Indian transport (transXBT) takes into account the observed vertical structure and assuming an upper layer of 150m on the Pacific side cannot be wrong enough to explain a difference of 5 Sverdrups. Note that the late 1997 westward transport increase in the Indian ocean differs by 12 Sverdrups with the decrease estimated on the Pacific side at that time. The Indian and Pacific series appear out of phase in 1996-1997-1998. One can certainly expect some shift in time between the Indian and the Pacific transports because of the connection time via the Indonesian waters. It also makes sense that this shift is neither a systematic lag nor lead because the residential time in the Indonesian waters varies with ENSO. Nevertheless, the differences between the two ocean transports are definitely too big to be reasonable. If the Indonesian seas are viewed as a reservoir over a surface of 10°*10°, an excess of one Sverdrup of inflow over the outflow during one month would make the sea level rise by more than one meter. One has to find another mass source that explains why the Indian estimate is so different from the Pacific estimate.

Figure 5 presents a zoom over the Indo-Pacific region of the SLA data set showing the landmask and the various possible water pathways. Because the hydrographic values are relative to the 400m level, shallow seas are masked. Even though the passage South of New-Guinea is not open down to 400m, we computed the geostrophic transport variations across line (2) in order to find out if some of the Indian transport variations could come from these shallow seas. This is not the case. Even when assuming a variable upper ocean thickness between 150m and 400m that could favor larger transports, the anomalies across section (2) are always smaller than one Sverdrup. Section (3) is the other possible entry of Pacific waters into the Indonesian seas. Similar small values are found across this section. They are negligible compared to the transport variations across section (1). So the difference between the Pacific and the Indian transport estimate (solid curve in Fig. 6) must be compensated by some other waters. It is found that the South-to-North geostrophic transport across section (5) explains this difference to a good extent. The Indian estimate is significantly influenced by exchanges with the South.

In summary, one would need continuous monitoring of the vertical temperature and salinity profiles across the various Indonesian channels to estimate accurate transports of the Throughflow. Such data set is not available. So using sea level data not too close and not too far from the coasts and applying the geostrophic approximation is still a useful approach today. It can be done either on the Pacific or on the Indian side. Because hydrographic measurements have been performed since 1983 on the Indian side, we a priori intended to use the Indian estimate to study the

impact of the Throughflow on ENSO. This estimate is certainly useful to correct a model of the Indian Ocean that has closed boundaries (paper in preparation). However given the fact that the Indian transport involves exchanges with waters that do not come only from the Pacific, transport across section (1) is the appropriate estimate to be used for correcting the closed Pacific model of this paper.

4 - The model and the control run

The model used in this study is an Intermediate Coupled ocean-atmosphere Model (ICM) of the tropical Pacific. It simulates interannual anomalies relative to a prescribed climatology. The ocean model, named Trident (code provided by Dr. Boulanger), has a dynamic component and a thermodynamic component. The SST anomalies are governed by the zonal, meridional and vertical anomalous heat transports. Trident is thus similar to the ocean component of the ICMs presented in Zebiak and Cane (1987) or in Cassou and Perigaud (2000). Compared to these models, more accurate numerical schemes have been implemented including a finer grid resolution and a landmask, and the climatological fields as well as the various parameterizations have been re-estimated to better fit observations during the 70-s and 80-s. Trident driven by observed wind anomalies over 1992-1998 agree well with satellite and in situ data (Boulanger, 2000; Boulanger and Menkes, 2000). The atmospheric component is a statistical model named Astat, which is the atmospheric component of the "Tsub.Astat" model presented in Cassou and Perigaud (2000). Astat is constructed by Singular Value Decomposition between the FSU (Florida State University) wind stress and the CAC (Climate Analysis Center)

SST anomalies between 1970 and 1983. Astat model forced by the observed SST anomalies over 1980-1998 reproduces well the ENSO variations of the wind, including the zonal component in the equatorial central Pacific and the meridional component in the Inter-Tropical and South Pacific Convergence Zones (ITCZ and SPCZ). Trident is coupled to a statistical atmosphere rather than to the atmospheric component of the Cane and Zebiak's model to avoid errors for both wind components in the eastern Pacific.

For the present study, we choose to retain only one vertical mode in the baroclinic ocean although more than one mode are needed to account for the totality of the actual Indonesian Throughflow variations. Our choice is justified when considering the large uncertainty of the Throughflow transport estimates found in the literature, whether it is from data or from models. Indeed studies focusing on the upper layer ocean changes, including recent studies (Vershell et al, 1995; Potemra, 1999), are also based on a single mode. In addition, when performing the experiments with prescribed Throughflow transport at the western boundary of the model, retaining a single mode avoids arbitrary projections of the observed sea level information on the vertical. With a phase speed equal to 2.50 m/s, an upper layer thickness equal to 150m and a Rayleigh friction of a 12 months time decay, the Trident.Astat coupled model reproduces SST oscillations every 3 to 5 years like in Cane and Zebiak's model, but the behavior is different and the mechanism of equatorial heat content recharge by the off-equator involved in sustaining the coupled oscillations rather ressemble the one simulated by "Tsub.Astat" (Cassou and Perigaud, 2000).

The first forced experiments consist in forcing the model by observed wind stress anomalies from January 1980 to July 1998 with the closed boundary condition. The experiment used as the control run (CR) for this paper is initialized from rest in 1970 and forced by the stress anomalies named Astat(CAC). They are the stress anomalies estimated by Astat from the observed SST anomalies. A second experiment named run.FSU is initialized from rest in 1961 and forced by the stress anomalies derived from the FSU non-detrended data set. Model outputs (SL, SST and wind stress anomalies) are monthly averaged. Maps of their variability over 1980-1998 are presented for the control run (Fig.7) and compared with observations (Fig. 8). Attention is first focused on this comparison, because reproducing the correct patterns of the oceanic and atmospheric signals in the forced context is a challenging step which is necessary before performing coupled experiments. Then, we validate the time series of spatially averaged quantities commonly used like the Niño3 index and examine their sensitivity to the wind used to force the model.

The simulated and observed sea level variability maps (Fig. 7a and 8a) present the expected patterns with maxima along the equator east of the dateline and in the off-equatorial regions west of the dateline, but they also display some discrepancy. Compared to the observed maxima, the simulated maxima are stronger in the Southwest (12 cm compared to 8 cm), weaker in the eastern equatorial region (6 cm compared to 8 cm) and located significantly east and south of the observed maximum in the Northwest region (near 170°E, 5°N compared to 130°E, 10°N). Also, the minimum of variability in the central Pacific is located to the East of the dateline where it is observed. Part of this discrepancy is explained by the fact that the

model has one baroclinic mode only. A minimum of 4 modes is suggested in (Dewitte, 2000) to reach the skill of an Ocean General Circulation Model in reproducing the sea level variability. But even with four modes or with OGCMs, the minimum of variability is often located to the east of the dateline. Other factors, like the fact that the model overestimates the SLA due to reflected equatorial waves in comparison of the wind-driven ones (see Perigaud and Dewitte, 1996), explain this deficiency. It is crucial to reduce this deficiency as much as possible in a forced context, because the coupling which is strong in the eastern Pacific tends to displace the minimum even more to the East. Moreover the strength and duration of the warm events simulated by the coupled model crucially depend on the location of this minimum. We come back on this issue in Section 6.

The simulated and observed SST maps present strong similarities (Fig. 7b and 8b). The model reproduces the observed patterns of variability, including the presence of two maxima, one offshore slighted south of the equator with a maximum of about 1.3°C at 120°W, and the other one along the Peruvian coast with an amplitude of about 1.8°C. The agreement between the model and the data is indeed quite remarkable.

The variability of the zonal (TX) and meridional (TY) wind stress simulated by the control run is compared here to the observed anomalies Astat(CAC) used to force Trident in this control experiment. For TX (Fig. 7c and Fig.8c), the regions of intense anomalies are located on the equator between 170°E and 120°W, and between 10°S and 5°N. The model simulates the maximum between the dateline

and 160°W slightly south of the equator. The fact that the model places the wind maximum close to the correct location is another significant advantage of the Astat model compared to the Cane and Zebiak's atmosphere (see Perigaud and Dewitte, 1996). Values are weaker though for the model than for the data (0.18 dyn/cm^2 versus 0.24 dyn/cm^2). ICMs often simulate an amplitude too weak in the forced context and it is common to correct for this weakness by choosing a coupling coefficient larger than 1.0 when performing coupled experiments (the coefficient is 1.645 in the Cane and Zebiak's model).

For TY (Fig. 7.d and 8.d), the main patterns are reproduced by the model, with the highest values between 180°E and 110°W, north of the equator and south of 10°N. The maximum in the North is located in the central Pacific (near 140°W and 5°N), the maximum in the South is weaker and in the West. Contrary to the zonal component, the meridional wind has stronger values for the model than for the data (0.20 dyn/cm^2 versus 0.18 dyn/cm^2). Similar characteristics are found for the two wind components simulated by "Tsub.Astat" and because both play an important role in the simulated ENSO, the coupling coefficient must be chosen close to 1.0 in order to reproduce mechanisms that are not too far from reality. In the present paper, the coupling coefficient (which is applied in the computation of the wind stress outputs of the forced experiments) is equal to 1.0.

One may question the robustness of this validation because the observed winds are actually obtained from observed SST converted into wind stress. As illustrated on Fig.9, the agreement with the FSU observed stress is good for both components in the central Pacific. Note that the FSU stresses used here have not

been detrended like the stress used to force the Cane and Zebiak's model because since 1980, most of the ships are equipped with anemometers and the low-frequency trends of the FSU winds could be real. Discrepancies between FSU and Astat(CAC) winds are observed in the Northwestern Pacific (Fig, 9d). In order to examine how this discrepancy affects the control run, the model outputs generated by run.FSU are added to Fig. 10 which allows further validation of the control run.

Fig. 10 illustrates that the model reproduces the observed indices between 1980 and 1998 really well. The biggest disagreement between the control run and the data is found in sea level in the western Pacific in 1983-84. The control run simulates a trough of 15m whereas a trough of 10m is observed (Fig. 10a). Obviously, this misfit is due to the fact that the Astat(CAC) stress has an error. It is found that the error is not due to TX, but to TY which, in 1983, does not detect a strong enough southward displacement of the ITCZ (check Fig.9b). The strong TY anomaly of FSU in 1983 is associated to an anticyclonic curl which, given the cyclonic curl associated with TX, explains why the signal simulated in run.FSU is less negative than in the control run. The TY anomaly observed by FSU in 1983 is the strongest of all since 1980. Note that in 1997-98, it is TX which is the strongest of all and then, the 17m sea level trough observed by the satellite is as strong as in the control run (19m) or in run.FSU (14m). In the eastern Pacific (Fig. 10b), the the control run does not have an error in 1983 as large as in the West. For both experiments, the first two events are slightly overestimated by the model, whereas the last two are slightly underestimated. Overall between 1980 and 1998, the agreement is good, the control run and data are correlated by 0.79, they have an rms

difference of 4m in the West and 3m in the East. The control run also reproduces the observed SST and TX anomalies remarkably well (Fig. 10cd). Correlations with observations are respectively 0.87 and 0.91 and rms differences are 0.5°C and 0.006 Pa. The agreement is of similar quality for run.FSU.

In summary, the control run reproduces the sea level, the SST and the wind stress variability quite well over 1980-1998. Relatively speaking, the biggest model deficiency is found in the sea level. The minimum of variability is not reproduced where it is observed at the date line, and the amplitudes of the anomalies in the western and eastern Pacific do not always match the observations. Part of this discrepancy is due to errors in the wind used to force the control run. But replacing this wind by the FSU wind does not significantly improve the simulations, except for the sea level in the western Pacific in 1983. In addition to the wind forcing, the sea level is affected by the wave-reflection at the boundaries. The closed boundary conditions verified by the model ignore the mass inflows and outflows that take place across the western boundary because of the Indo-Pacific oceanic connection. Let us now try and estimate such flow variations.

5 –Estimation of the flow across the model western boundary due to the Indo-Pacific connection.

The baroclinic model is decomposed in Rossby and Kelvin components like in Cane and Patton (1984). To verify the conditions of full reflection at the western boundary, the model integrates the zonal transport due to the Rossby signal between

20°S and 20°N, and determines the Kelvin amplitude that warranties no inflow nor outflow across this boundary. We have seen in Section 3 that sea level data can be used to estimate the geostrophic transport at the western boundary of the model across the section where the boundary is open in reality. We can now use the model outputs to estimate the transport (Rossby+Kelvin) across this part of the boundary which is due to the wind-driven-propagated-and-fully-reflected equatorial waves. If one assumes that the ocean model is perfect except for its closed conditions at the western boundary, the difference between the observed and the simulated estimates, named ITF, corresponds to the transport which is due to the oceanic connection of the Pacific with the Indian Ocean. Studying the impact of the Indo-Pacific connection on the ENSO signals simulated by our Pacific model then consists in prescribing the ITF inflow-outflow variations at the western boundary, meaning that, at each time step, the ITF correction is added to the value of the Kelvin wave at the western boundary obtained by the wind and the full reflection of the incoming Rossby signal. So let us first examine the model transport and then determine the ITF correction.

The 1980-1998 time series of the geostrophic zonal current anomalies are derived from the simulated sea level following the same method as for the observations in section 3. In fact, with the model SLA, we were able to verify that this method gives the same zonal current anomalies as the baroclinic currents provided by the model. Computations were done for the control run and for run.FSU in order to examine the part of the signal which could be due to wind error. The transports in Fig.11a correspond to the integration of the current

anomalies between 2.5°N and 7.5°N at 130°E like in Fig. 3b. Other latitudinal bands between 0° and 10°N and other longitudes between 130°E or 140°E have been tested. Transport estimates then slightly differ in amplitude and time, but the results derived by prescribing the ITF in the forced context (section 6) are not much sensitive to the extent nor to the position of the ITF section. On the contrary, results in the coupled context are significantly affected, and the section which best improves the coupled SST, wind and SLA, is the [2.5°N-7.5°N] section at 130°E (paper to be submitted). Here, results in Fig.11 and after are presented for this section.

The strongest transport anomalies simulated by the control run are to the West in late 1982- early 1983, in 1987, and in 1997 (Fig.11a). This is because the integration of the currents between 2.5°N and 7.5°N privileges the Rossby flow relatively to the Kelvin component which is centered at the equator. As expected, the Rossby currents in the western Pacific are westward and the strongest during the mature phase of the El Niño events. But each event is unique. Note that in late 1992 – early 1993, after the termination of the relatively mild event, both experiments simulate an eastward anomaly which is the strongest of all. The following years 1993 to 1998 correspond to the biggest scatter between the two model experiments and the data. It is striking in Fig.11a that the observed transport significantly differs in amplitude and phase with the simulated transports whereas both simulations agree to a large extent. So wind error is not the main reason why the observed transport differs from the model, the transport difference (data – model) is possibly representative of the Indo-Pacific connection.

The transport difference for the control run, the ITF correction, is presented together with the ENSO signal as observed with the SST Niño3 index (Fig. 11b). The correlation between the two signals is positive (0.65). Note that the observed transport itself is also positively correlated with ENSO, eastward transport anomalies being associated with warm events and westward with cold. The correlation is 0.29, close to the value of 0.31 found by Murtugudde et al, 1998. So, the ITF correction is more positively correlated than the observed transport. This is because warm events trigger westward upwelled Rossby waves that reflect at the western boundary to erode the warm growth, the model transport is negatively correlated with ENSO (–0.76). Even though the ITF correction is more significantly positively correlated to ENSO than the transport itself, what matters to make some progress in understanding the coupling between the Indo-Pacific connection and ENSO is precisely the shift in time between the two series. The sign of the shift indicates whether the ITF changes are primarily governed by the equatorial SST of the Pacific via the wind forcing, or whether it is rather the SST changes that are influenced by the ITF fluctuations via oceanic transport. The positive peaks of the ITF in Fig. 11b are clearly leading the SST peaks by 6 to 12 months. Actually, the ITF is leading the SST almost all the time over 1980-1998, the maximum correlation (0.72) is obtained for a 2 month-lead in the ITF. So the ITF correction appears to have a triggering role in the warm and cold events observed over 1980-1998. Of course, the ITF corrections themselves are also a response to atmospheric variations, probably they involve the global atmospheric patterns and the slower oceanic adjusments of the off-equatorial Pacific and the Indian Oceans as proposed by

Godfrey (1989; 1996) or Wajsowicz (1995). We come back on this issue in section 6. Even if the ITF leads the SST, the lead is far from constant. Fig. 11b shows large differences in amplitude between the ITF and SST associated peaks. Other processes are taking place at the same time. The SST Niño3 is coupled with the wind anomalies in the central equatorial Pacific and both keep changing and influencing each other, even if there was no Indo-Pacific connection. The ITF correction also keeps changing in time, probably in response to larger-scale variations. All these processes are constantly evolving from one event to the next one and make each event unique. The ITF rise is not leading the SST in 1981-82 whereas it is well in advance for the other events. The 1993 to 1995 period is quite remarkable with its two small ITF peaks that happen a few months prior and after the two aborted warm events of this period. This is all the more remarkable as this period is covered by the satellite when the ITF estimate is the most reliable. Finally for the last event, the ITF started to rise as early as two years prior to the SST warming. Each event need to be examined separately with appropriate coupled experiments (paper to be submitted). Before, one needs to initialize the model with realistic conditions at the western boundary. So one can examine the ITF role on the ENSO simulated in the forced context.

6 - Forced simulations with a prescribed ITF at the western boundary

In this section, the values of the ITF corrections are prescribed at the western boundary during a model experiment named run.ITF. Even though the model undergoes some inflow-outflow at its boundary, it does not loose mass nor drift

away towards warm or cold states during its time-integration, because the prescribed values are anomalies and have a zero mean over the period. Except for the western boundary condition, the configuration of the model is identical to the control run. Results of the two experiments are compared in this section and validated with the observations that have not been assimilated in the model.

In a forced context, the impact of prescribing the ITF on the baroclinic ocean is fully explained by the correction of the Kelvin amplitude at the western boundary. It means that the amplitude of the thermocline correction is linearly dependent on the ITF with a systematic lag as it propagates to the East. It reaches the eastern boundary in almost 3 months without being much damped by the friction which has a 12 month decay. It is known that the thermocline displacements strongly affect the SST changes in the eastern Pacific. Other terms such as the zonal advection of warm waters from the western Pacific (see Picaut et al, 1996; Jin, 1999) also play a role in ENSO. So does the local convergence of Ekman currents, but in the Niño3 region, the thermocline term is the dominant one among all the terms involved in the SST equation (the reader can check the time series of the various terms involved in the SST changes simulated in the forced experiment presented in Fig. 17 of Cassou and Perigaud, 2000). So one can anticipate that prescribing an inflow (outflow) at the western boundary will create positive (negative) SLA, i.e. deepening (shoaling) of the thermocline in the eastern Pacific that induces a positive (negative) correction in the Niño3 SST index a few months after. In the forced context, an ITF inflow/outflow anomaly is thus expected to modify the wind anomaly in the central Pacific with a westerly/easterly correction.

Details in Figure 12 confirm that this is how the ITF correction affects the simulated sea level, SST and wind anomalies. In particular, the SST negative anomalies between late-1983 and mid-1986 correspond to the outflow prescribed between early-1983 and late-1985. Similarly, the warmer SST anomalies in mid-1987 happen a few months after the peak of ITF inflow in 1986-1987. But the striking result of Fig. 12 is that the impact on the simulated fields is little. The sea level is affected by no more than 5 cm (Fig. 12ab). Note that in the east and in the west, the correlation is slightly degraded by the ITF (0.73 instead of 0.79). This is because the sea level of the ITF experiment is lagging the control run by a few months. But the ITF does not significantly reduce nor improve the model sea level in this forced experiment, the rms differences remain equal to 4m. Prescribing the ITF does not change much the Niño3 SST index either, the differences are smaller than 0.5°C (Fig. 12c). This is consistent with the small impact found in Murtugudde et al (1998). Indeed, even without any reflection at all, Trident forced by observed winds reproduce reasonably well the Niño3 index observed during the recent event (Boulanger and Menkes, 2000). Over 1980-1998, the ITF slightly degrades the correlation (0.84 instead of 0.87), the rms difference remains equal to 0.5°C. Finally (Fig. 12d), prescribing the ITF increases the amplitude of the wind peaks simulated in 1987, 1988, 1992 and 1997 closer to the observed ones. Overall, the ITF slightly degrades the correlation (0.88 instead of 0.91) and the rms difference remains smaller than 0.01Pa. Given the level of uncertainty in sea level, SST and wind data, the impact of the ITF on these indices is indeed negligible.

These results are likely to be specific, though, to the forced context. The weak differences between the two experiments are explained by the fact that the ENSO signal in the Pacific is primarily governed by the zonal wind stress anomalies which are identical in these two experiments. But in the coupled context, very slight changes of the thermocline can drastically affect the results by putting the model in a self-sustained oscillation mode or in a stable regime. One of the critical aspects that controls the coupled behavior is the position of the minimum of sea level variability as a function of longitude along the equator. As said in section 4, the control run does not locate it at the dateline where it is observed, but in the central Pacific. Fig. 13 shows that prescribing the ITF significantly reduces this model deficiency. It also reduces the simulated variability in the West and increases it in the East, in better agreement with observations. This positive impact is an additional argument indicating that our ITF estimate corresponds to an actual process missed by the model when the boundary is closed. Let us explain this important result. In both experiments, the simulated minimum is located to the east of the observed one because the model overestimates the variability due to free and reflected waves in comparison to the wind-driven ones. This has been demonstrated in Perigaud and Dewitte (1996) by testing various friction and reflection coefficients. Let us now explain why adding the ITF values displaces the minimum to the West. In the case of a warm event at a given time in both experiments, the sea level anomaly forced by a westerly in the central Pacific is positive in the East and negative in the West, and the reflection of the Rossby waves into the negative Kelvin waves contributes to even more negative in the

West and to less positive in the East. So, with the same wind, prescribing an eastward ITF correction corresponds to reflecting less negative anomalies, the signal is therefore less negative in the West and after propagation it is more positive in the East, thus decreasing the variability in the West, increasing it in the East, and locating the minimum less to the East of the forcing region. Similar results are found in testing the sensitivity of a global OGCM to the opening of the Indo-Pacific boundary (Lee, personal communication).

Another critical quantity involved in the coupled behavior is the zonally averaged sea level anomaly because the equatorial ocean gets recharged meridionally by the off-equator (Jin, 1997; Cassou and Perigaud, 2000). The time series of this quantity are presented for the two experiments and the observations over 1980-1998 (Fig.14a). The observed rms amplitude over 1980-1998 is 2.7 cm. The model with closed boundary has much weaker variations. The ITF has a significant impact on this signal in increasing the rms amplitude of the simulated signal from 1.3 cm to 2.5 cm. Also, the strong anomalies observed in 1982, 1983-84, 1988-89, 1991-92 and 1996-97 are fairly well reproduced by the ITF experiment. Note that like in fig. 12a, the signal simulated with the ITF tends to lag the observed signal. This is why ITF reduces the rms difference with observations from 2.1cm to 1.8cm only and does not improve much the correlation (from 0.68 to 0.69).

As expected, the difference between the run.ITF and the control run is well correlated with the ITF (0.75) and the ITF is leading the sea level correction (Fig.14b). The best correlation (0.77) is obtained for a 2 month lag in the simulated

sea level correction. In addition, Fig.14b shows that the difference between the two closed boundary experiments is small in comparison of the correction brought by the ITF. The experiment forced by FSU simulates a basin-averaged sea level which is very similar to the control run and agrees poorly with the observed level. A surprising result is found by comparing the observed sea level with the ITF (Fig.14c). The two time-series are positively correlated (0.72), but the ITF does not lead the basin-averaged sea level, it is the latter which leads the ITF. The correlation is equal to 0.78 with a lead of 2 months for the observed sea level. Thus in reality, the ITF does not control the basin-averaged equatorial sea level like in this forced experiment. This detail has important consequences for ENSO forecasts and is re-examined in the paper reporting the results of the coupled experiments. It is also consistent with the fact that what drives the ITF corrections involve large-scale connections of the equatorial Pacific with the rest of the world ocean.

Finally, let us examine the zonally averaged SLA outside of the equator. As expected, for both experiments, the model agreement with the data is poorer than in the equatorial band. In the North (Fig. 15a), the correlation between model and data is improved by the ITF, but not much (0.47 for the control run, 0.42 for the ITF experiment). This is because the North has winds which vary a lot all along with the ITCZ. Indeed, it is found that the Astat(CAC) wind misses the wind variability which is not retained by the SVD and the experiment forced by FSU recovers pretty well the level changes of the North. In the South (Fig. 15b), the ITF improves the correlation between the model and the data from 0.21 to 0.44. It improves the South more significantly than the North because the South level is relatively more

dependent on its boundary conditions than on its wind. Indeed, it is found that run.FSU does not simulate the South better than the control run. Observations reveal that the signal in the South is dominated by a regular increase between 1983 and 1997. This trend is completely missed by the two model experiments which have their boundary closed. It is quite remarkable that prescribing the ITF introduces a trend in the South which also corresponds to a regular increase between 1983 and 1997. It appears that the observed interdecadal trend in the South could be associated with the Indo-Pacific oceanic connection. This could well take place in reality. It needs more investigation, all the more as it is at the equator and South of it, where the cold tongue is located, that the strongest coupling between the ocean and the atmosphere takes place.

7 – Summary and perspectives

This study examines the impact of the Indo-Pacific oceanic connection on ENSO using Indian and Pacific sea level data between January 1980 and June 1998 and using an ocean-atmosphere model of the tropical Pacific. This first paper is focused on the estimate of the flow across the Pacific western boundary which is associated with the Indo-Pacific oceanic connection and on its validation with the ENSO signals simulated by the model in a forced context.

The Indonesian Throughflow variations are known to be correlated with ENSO, the transport from the Pacific to the Indian ocean decreasing during warm events and increasing during cold events. This is confirmed by all the estimates

presented in this paper. However, the correlation between the Throughflow variations and the SST Niño3 time series is not high (0.3) because the transport is not linked to the equatorial Pacific ENSO only, it is influenced by other factors in the off-equatorial Pacific and Indian Oceans as well. Indeed one needs a better understanding of these other factors to make progress in ENSO forecasting. This appeals for more accuracy in the observed transport, but also for more data acquisition (such as current meters distributed on the vertical across the opening of the Pacific Northwestern boundary) and for model improvements (such as adding baroclinic modes). This study is a first investigation of the role of the Throughflow on the coupled ocean-atmosphere. Given the data uncertainty and the extreme sensitivity of coupled models to initial conditions, parameterizations and off-equatorial processes, our choice is to rely on sea level data, in particular the accurate TOPEX/Poseidon data set, and on models with physics as simplified as possible.

It has been mentioned several times in the literature that a proxy to the Throughflow variations is the difference between the Pacific and the Southeastern Indian sea levels. The new result found here is that the geostrophic transport variations across 130°E [2.5°N-7.5°N] in the western Pacific match well such a proxy. On the other hand, they do not match well the geostrophic transport variations estimated in the Indian Ocean across the section between NW Australia and Java because the latter involve exchanges with the Southern Indian Ocean in addition to the Pacific. So the impact of the Throughflow on the Pacific ENSO is studied here with the transport computed on the Pacific side. The ITF transport due to the Indo-Pacific connection is then obtained by removing the component simulated by the

wind-driven and fully-reflected equatorial waves of the Pacific. It is found that the ITF transport correlates better with the SST Niño3 index (0.7) than before the removal (0.3) and is not much sensitive to the differences between the two wind forcings that were tested.

Simulations obtained when prescribing the ITF at the western boundary of the model to correct for its closed boundary confirm that the ITF estimate is valid. It reduces the model misfit with data for quantities that are away from the western boundary. In better agreement with data, the ITF weakens the sea level variability in the West, increases it in the East and puts the minimum of variability to the West of where it is simulated with closed boundary conditions. This is a very interesting case to examine in the coupled context, because all the tests performed with ICMs produce oscillations with stronger amplitude in the East when the minimum is displaced to the East and not to the West.

In addition, the ITF correction significantly amplifies the simulated basin-averaged sea level changes of the equatorial Pacific in good agreement with observations (correlation of 0.7). As a result of the forced approach though, the sea level is lagging the ITF whereas in fact, observed sea level leads the ITF by a few months. The basin-averaged equatorial level is not linked to the equatorial zonal wind (at least not within the simplified context chosen here). It rather depends on the exchanges with the off-equatorial Pacific and with the Indian Ocean. Interestingly, it is found that the interdecadal trend observed in the South is partly recovered by prescribing the ITF. Of course, because of our simplified modeling

context, the model-data agreement remains poor off-equator (correlation of 0.4). It is certainly more efficient to initialize the model with sea level data like in (Perigaud et al, 2000) than with the outputs of the ITF experiment before performing ENSO forecasts. Nevertheless, no matter how good the initial conditions are, the realiability of a predictive model depends on its ability to simulate realistic mechanisms during the coupled experiment itself. The models used for ENSO forecasts ignore the mechanisms associated with the Indo-Pacific oceanic connection. The ITF has a negligible impact on the SST Niño3 in these forced experiments because the wind is controlled by observations, but there is no such control in the coupled context. Aware of the great sensitivity of the coupled simulations and knowing that the ITF is leading the SST Niño3, are we still sure that we can continue ignoring the ITF when we try and make forecasts? One cannot answer this question without performing the coupled experiments. Observations indicate that for each event, the ITF does not have the same phase difference nor amplitude modulation relative to the SST Niño3 index. Each event is rather a unique combination of coupled equatorial/off-equatorial anomalies over the Pacific and the Indian oceans.

Acknowledgments

The research described in this paper was carried out by the Jet Propulsion Laboratory, California Institute of Technology, under a contract with the National Aeronautics and Space Agency. The authors thank Akiko Ayashi from the Jet Propulsion Laboratory for providing the processed and gridded TOPEX/Poseidon data, Dr. Gary

Meyers from CSIRO and Dr. Neville Smith from BRMC who kindly made available their respective analysis of subsurface temperature data along the South-eastern Indian XBT line or over the Indian and Pacific oceans. They also thank Dr. J.P. Boulanger who provided the code of the Trident model.

List of references

Boulanger, J.-P., The Trident Pacific Model, Part 1: The oceanic dynamical model and observations during the TOPEX/POSEIDON period, *Climate Dynamics*, revised version, 2000.

Boulanger, J.-P., and C. Menkes, The Trident Pacific Model, Part 2: The thermodynamical model and the role of long equatorial wave reflection during the TOPEX/POSEIDON period, *Climate Dynamics*, revised version, 2000.

Broecker, W. S., The great ocean conveyor, *Oceanography*, 4, 79-89, 1991.

Cane, M. A., and R. J. Patton, A numerical model for low-frequency equatorial dynamics, *J. Phys. Oceanogr.*, **12**, 1853-1863, 1984.

Cassou, C., and C. Perigaud, ENSO simulated with Intermediate Coupled Models And evaluated with observations over 1970-1998, Part II: Importance of the off-equatorial wind and ocean, *J. Climate*, in press, 2000.

Clarke, A., and X. Liu, Interannual sea level in the northern and eastern Indian Ocean, *J. Phys. Oceanogr., 24*, 1224-1235, 1994.

Delcroix, T., J.-P. Boulanger, F. Masia, and C. Menkes, GEOSAT-derived sea level and surface-current anomalies in the equatorial Pacific, during the 1986-1989 El Niño and La Niña, *J. Geophys. Res., 99*, 25093-25107, 1994.

Dewitte B. Sensitivity of an intermediate ocean-atmosphere coupled model of the tropical Pacific to its oceanic vertical structure, *J. Climate*, in press, 2000.

Fieux, M., R. Molcard and A. Ilahude, Geostrophic transport of the Pacific-Indian Oceans throughflow, *J. Geophys. Res., 101*, 12421-12432, 1996.

Godfrey, J. S., A Sverdrup model of the depth-integrated flow for the world ocean allowing island circulations, *Geophys. Astrophys. Fluid. Dyn., 45*, 89-112, 1989.

Godfrey, J. S., The effect of Indonesian throughflow on ocean circulation and heat exchange with the atmosphere, *J. Geophys. Res., 101*, 12217-12237, 1996.

Gordon, A., Interocean exchange of thermocline water, *J. Geophys. Res., 91*, 5037-5046, 1986.

Hirst A.C., and J.S. Godfrey, The role of Indonesian Throughflow in a global ocean GCM, *J. Phys. Ocean.*, Vol. 23, 1057-1086, 1993.

Jin F.F., An equatorial ocean recharge paradigm for ENSO. Part I: Conceptual model. *J. Atmos. Sci., 54*, 811-829, 1997.

Jin F.F., Thermocline and Zonal advective Feedbacks within the equatorial Ocean Recharge Oscillator Model for ENSO, *Geophys. Res. Lett.*, 26, 2989-2992, 1999.

Kindle, J., H. Hurlburt, and E. Metzger, On the seasonal and interannual variability of the Pacific to Indian ocean throughflow, paper presented at the Western Pacific *International Meeting and Workshop on TOGA COARE*, ORSTOM, Noumea, New Caledonia, 1989.

Meyers, G., Variation of Indonesian throughflow and the El Niño Southern Oscillation, *J. Geophys. Res.*, Vol. 101, No C5., 12225-12263, 1996.

Murtugudde, R., A. J. Busalacchi, and J. Beauchamp, Seasonal to interannual effects of the Indonesian throughflow on the tropical Indo-Pacific Basin, *J. Geophys. Res., 103*, 21425-21441, 1998.

Nof D., 1996: What controls the origin of tge Indonesian Throughflow?", *J. Geophys. Res.*, **101**, 12301-12314.

Perigaud C. and B. Dewitte, El Nino – La Nina events simulated with Cane and Zebiak's model and observed with satellite and in situ data. Part I: model and data comparison, *J. Climate*, 9 , 66-84, 1996.

Perigaud, C., C. Cassou, B. Dewitte, L.L. Fu, and D.J. Neelin, Use of data to improve Seasonal to Interannual forecasts simulated by Intermediate Coupled Models, *Mon. Wea. Rev.*, in press, 2000.

Picaut, J., M. Ioualalen, C. Menkes, T. Delcroix, and M. J. McPhaden, Mechanism of the zonal displacements of the Pacific warm pool: implications for ENSO, *Science*, **274**, 1486-1489, 1996.

Potemra J.T., 1999: Seasonal variations of upper ocean transport from the Pacific to the Indian Ocean via Indonesian straits, J. Geophys. Res., 29, 2930-2944.

Potemra J.T. and R.Lukas, 1999: Seasonal to Interannual modes of sea level variability in the western Pacific and eastern Indian Oceans, *Geophys. Res. Lett.*

Schneider N., The Indonesian Throughflow and the Global Climate System, *J. Climate*, Vol 11, No.4, 676-689, 1998.

Smith, N. R., An improved system for tropical ocean subsurface temperature analyses, *J. Atmos. Oceanic. Technol., 12*, 850-870, 1995.

Vershell, M., J. Kindle, and J. O'Brien, Effects of Indo-Pacific throughflow on the upper tropical Pacific and Indian Oceans, *J. Geophys. Res., 100*, 18409-18420, 1995.

Wajsowicz, R. C., A relationship between the interannual variations in the south Pacific wind stress curl, the Indonesian throughflow and the west Pacific warm water pool, *J. Phys. Oceanogr., 24*, 2180-2187, 1994.

Wyrtki K.: Indonesian Throughflow and the associated pressure gradient, *J. Geophys. Res.*, **92**, 12941-12946.

Zebiak, S. E., and M. A. Cane, A model El Niño/Southern Oscillation, *Mon. Wea. Rev.*, **115**, 2262-2278, 1987.

Figure Caption

Figure 1: (a) Mean sea level anomaly derived from Hdyn over January 1993-December 1996. Unit: cm. Dashed lines correspond to negative values; (b) Ratio of the RMS variability of Hdyn over the RMS variability of TP. The RMS are computed over October 1992 - March 1998. Dashed line corresponds to values smaller or equal to 1.

Figure 2: Time series of SLA derived from Hdyn (solid line) or from TP (dotted line) averaged over (ac) the western Pacific Ocean (135°E - 140°E, 0°-5°N); (bd) the southeast Indian Ocean (100°E - 120°E, 14°S - 8°S). (ab) are prior to correction and (cd) are after correction.

Figure 3: Time series of (a): SLA at 125°E-5°N (close to Davao) and at 122°E, 12°S (close to Darwin). (b): SLA difference (Darwin-Davao) in cm and zonal transport in Sverdrup across the section 130°E [2.5°N-7.5°N]. Sign is positive to the East.

Figure 4: Time series of (a) SLA at 105°E-8°S (South of Java) and at 110°E-20°S (NW of Australia). (b): Transports across the XBT line [105.5°E, 7.5°S to 33.5°S, 114.5°E] with the solid curve for (TransXBT) and the dotted curve for (Transhdyn) and transport across the zonal section 105°E [8°S-20°S] with the dashed line for (transSLA) .

Figure 5: Landmask of the SLA data set and passages in the Pacific and Indian Oceans across which transports in Fig.3, Fig.4 and Fig.6 are computed.

Figure 6: Time series of zonal and meridional transport. Sign is positive to the North. The plain curve represents the zonal transport difference between

the Pacific sections (1+2+3) and the Indian section 105°E [8°S-20°S]. The dashed curve represents the meridional transport across 20°S [105°E-115°E].

Figures 7: Maps of sea level, SST, zonal and meridional wind stress RMS variability over 1980-1998 simulated by the control run. Units are respectively: cm, °C and dyn/cm^2. Shaded areas correspond to the model topography.

Figures 8: Same as Figures 7 for observations.

Figure 9: Time series of zonal (TX) or meridional (TY) wind stress anomalies averaged over Niño4 (160°E - 150°W, 5°S - 5°N), NiñoN (180°E - 140°W, 1°N - 9°N), NiñoS (180°E - 140°W, 5°S - 15°S) or NinoWN (130°E –170°E, 1°N - 9°N). Plain line is the Astat(CAC) stress, dashed line is the FSU stress.

Figures 10: Time series of (a) SLA over Niño West (130°E - 170°E, 10°S - 10°N), (b) SLA over Niño3, (c) SST over Niño3, (d) zonal wind stress over Niño4. Solid line is for observations, dotted line for the control run, and dashed line for run.FSU.

Figure 11: Time series of (a) geostrophic transport across 130°E [2.5°N-7.5°N] derived from observed (solid line) or simulated SLA (dotted line is for the control run; dashed line for run.FSU), (b) ITF correction derived from the transport difference (data-control run) in Sverdrups and Niño3 SST index in °C (multiplied by 3 for the plot).

Figures 12: Time series of (a) SLA over Niño West, (b) SLA over Niño3, (c) SST over Niño3, (d) TX over Niño4. Solid line is for observations, dotted line for the control run, and dashed line for run.ITF.

Figure 13: RMS variability of SLA over 1980-1998 as a function of longitude along the equator.

Figure 14: Time series of SLA averaged over the equatorial Pacific (130°E - 80°W, 5°S - 5°N). (a) Plots are derived from observations (solid line), or from the control run (dotted line) or from run.ITF (dashed line). (b) SLA average difference between model outputs in cm and ITF transport in Sverdrup. (c) Observed SLA average in cm and ITF transport in Sv.

Figure 15: Time series of SLA averaged over the Pacific, from 130°E to 80°W (a) from 5°N to 10°N, (b) from 5°S to 10°S. Plots are derived from observations (solid line), from run.ITF (dashed line) or from the difference between run.FSU and the control run (dotted line).

REFERENCE SURFACE FROM HDYN - JAN 93-DEC 96 -

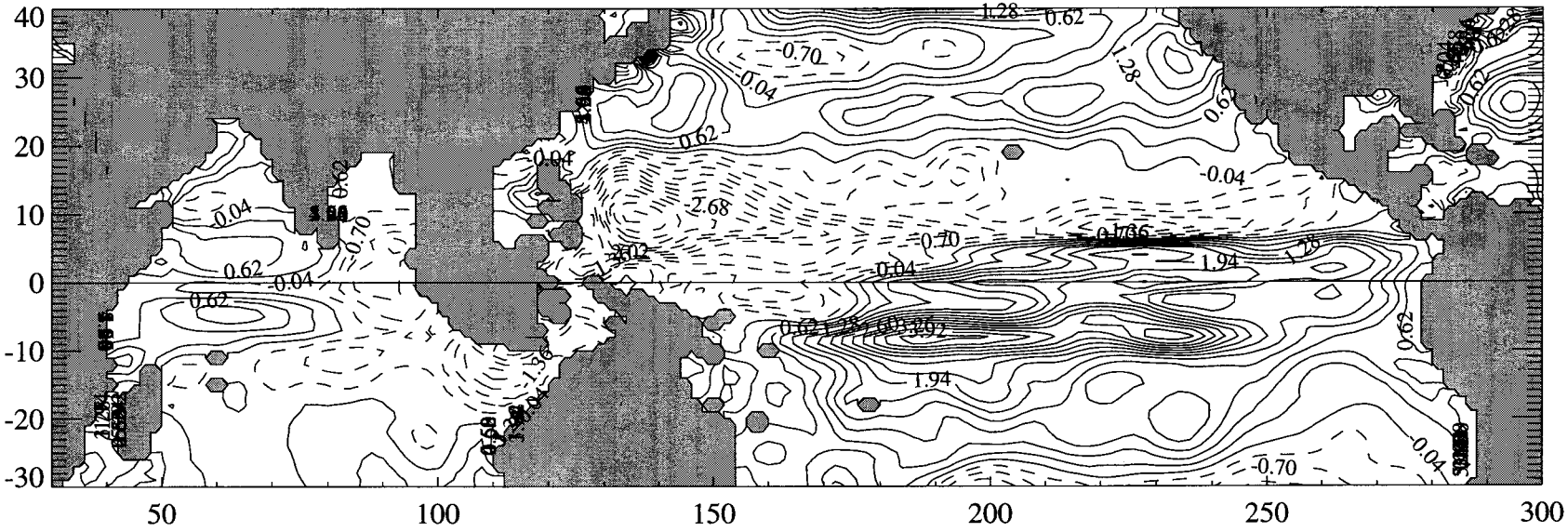

RATIO OF VARIABILITY BETWEEN TP AND HDYN - OCT 92-MARCH 98

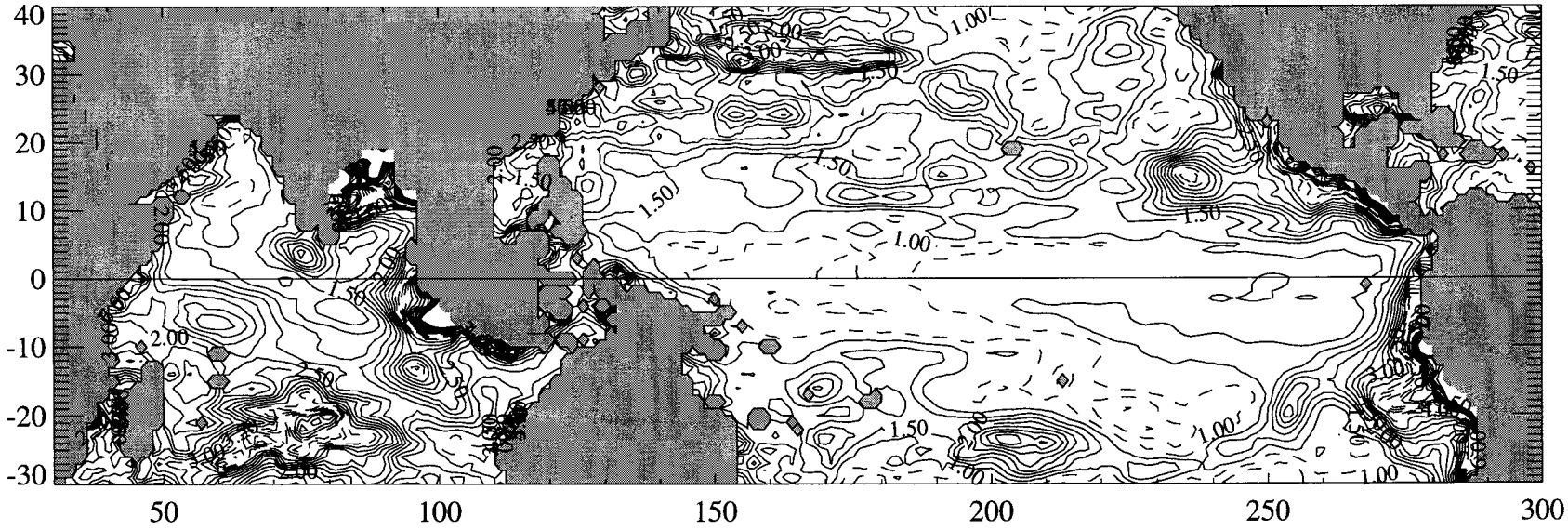

Fig. 1

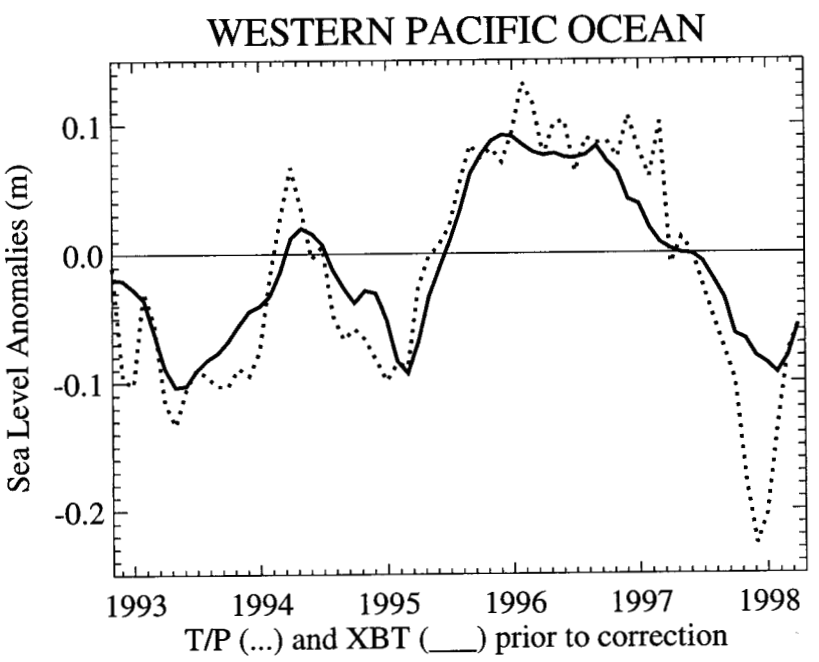
WESTERN PACIFIC OCEAN
Sea Level Anomalies (m)
0.1
0.0
-0.1
-0.2
1993
1994
1995
1996
1997
1998
T/P (...) and XBT (___) prior to correction

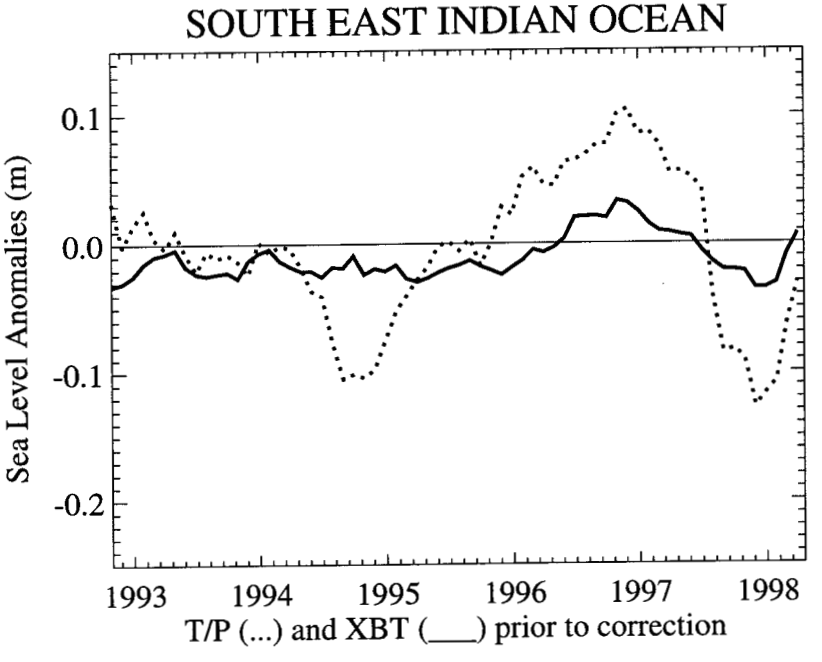
SOUTH EAST INDIAN OCEAN
Sea Level Anomalies (m)
0.1
0.0
-0.1
-0.2
1993
1994
1995
1996
1997
1998
T/P (...) and XBT (___) prior to correction

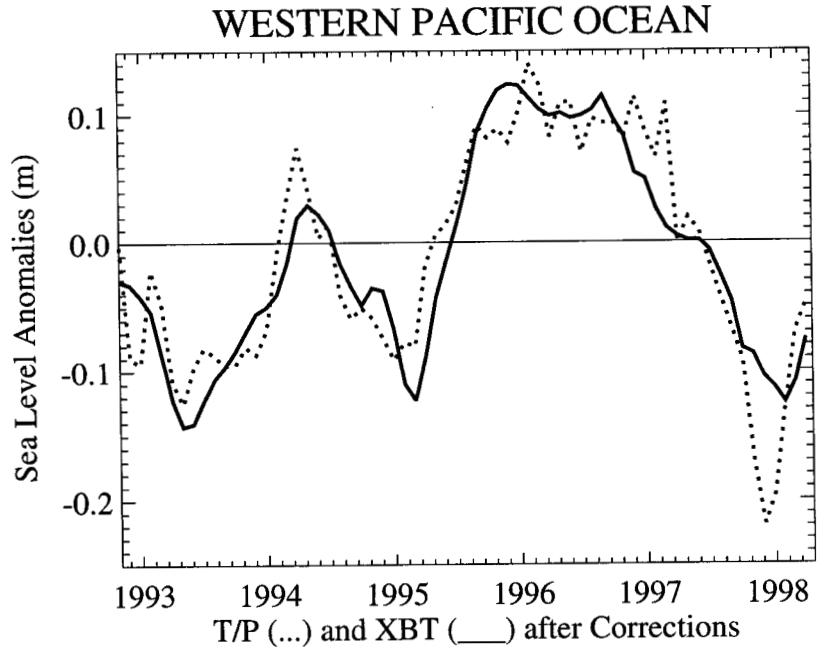
WESTERN PACIFIC OCEAN
Sea Level Anomalies (m)
0.1
0.0
-0.1
-0.2
1993
1994
1995
1996
1997
1998
T/P (...) and XBT (___) after Corrections

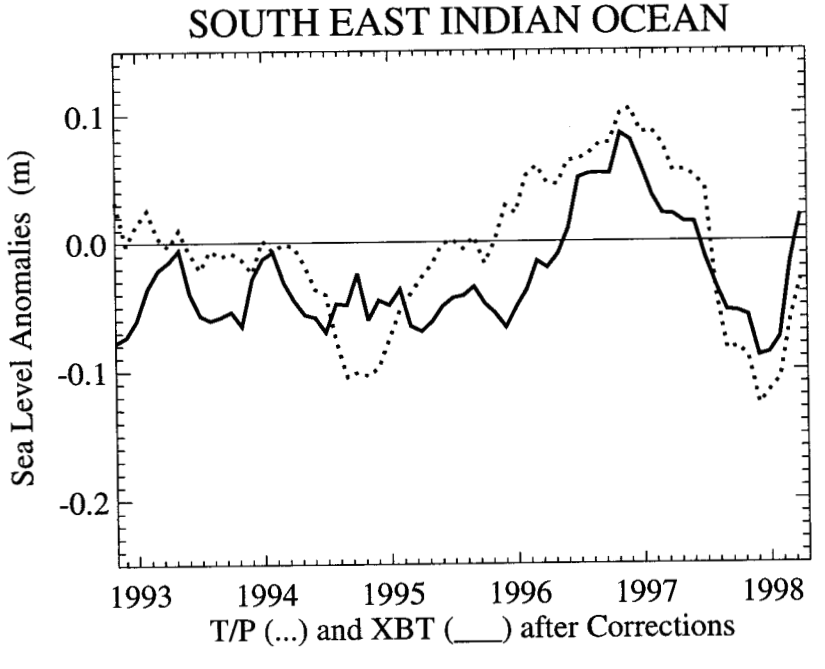
SOUTH EAST INDIAN OCEAN
Sea Level Anomalies (m)
0.1
0.0
-0.1
-0.2
1993
1994
1995
1996
1997
1998
T/P (...) and XBT (___) after Corrections

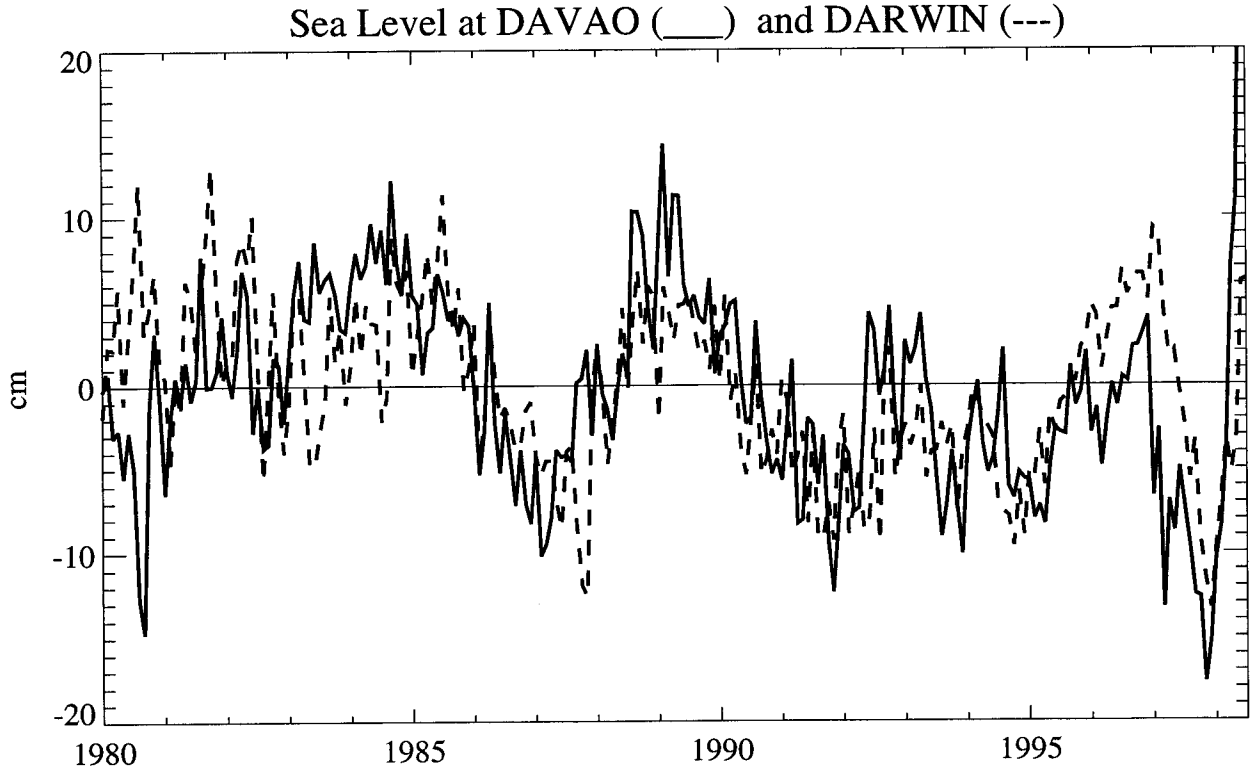
Sea Level at DAVAO (___) and DARWIN (---)
20
10
0
-10
-20
cm
1980
1985
1990
1995

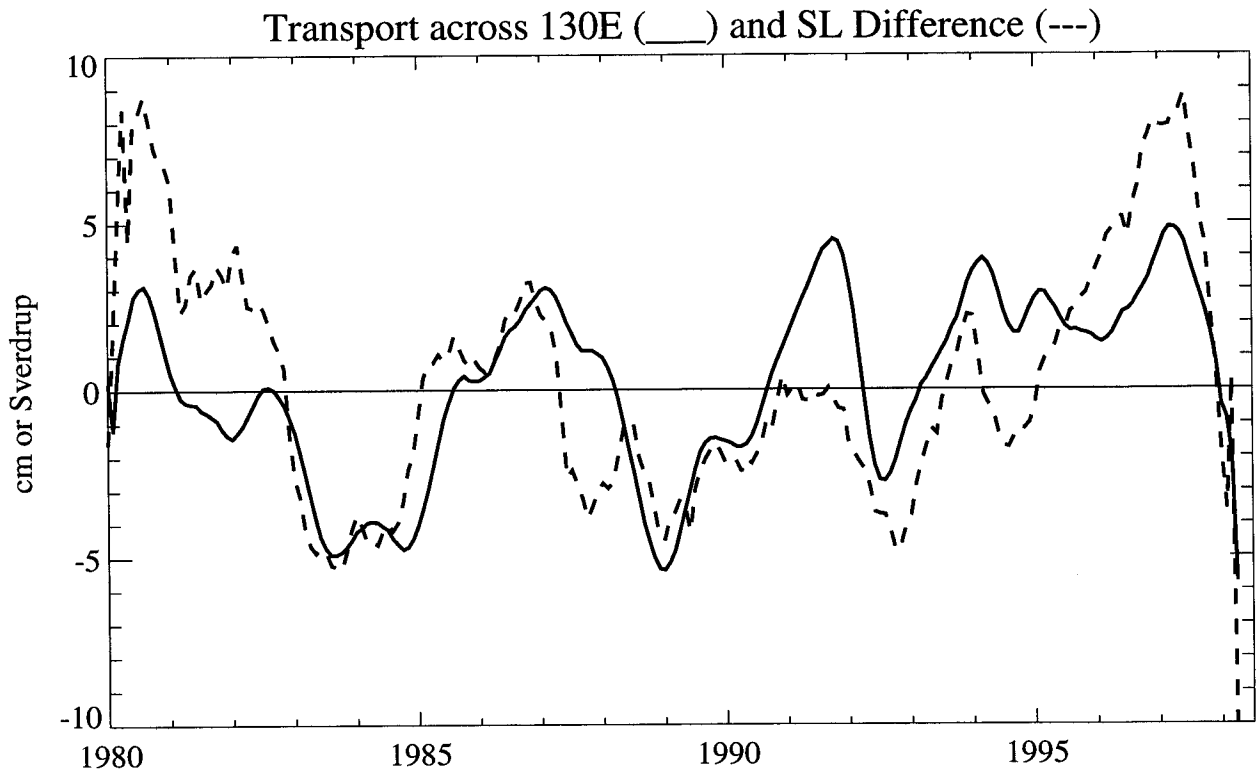
Transport across 130E (___) and SL Difference (---)
10
5
0
-5
-10
cm or Sverdrup
1980
1985
1990
1995

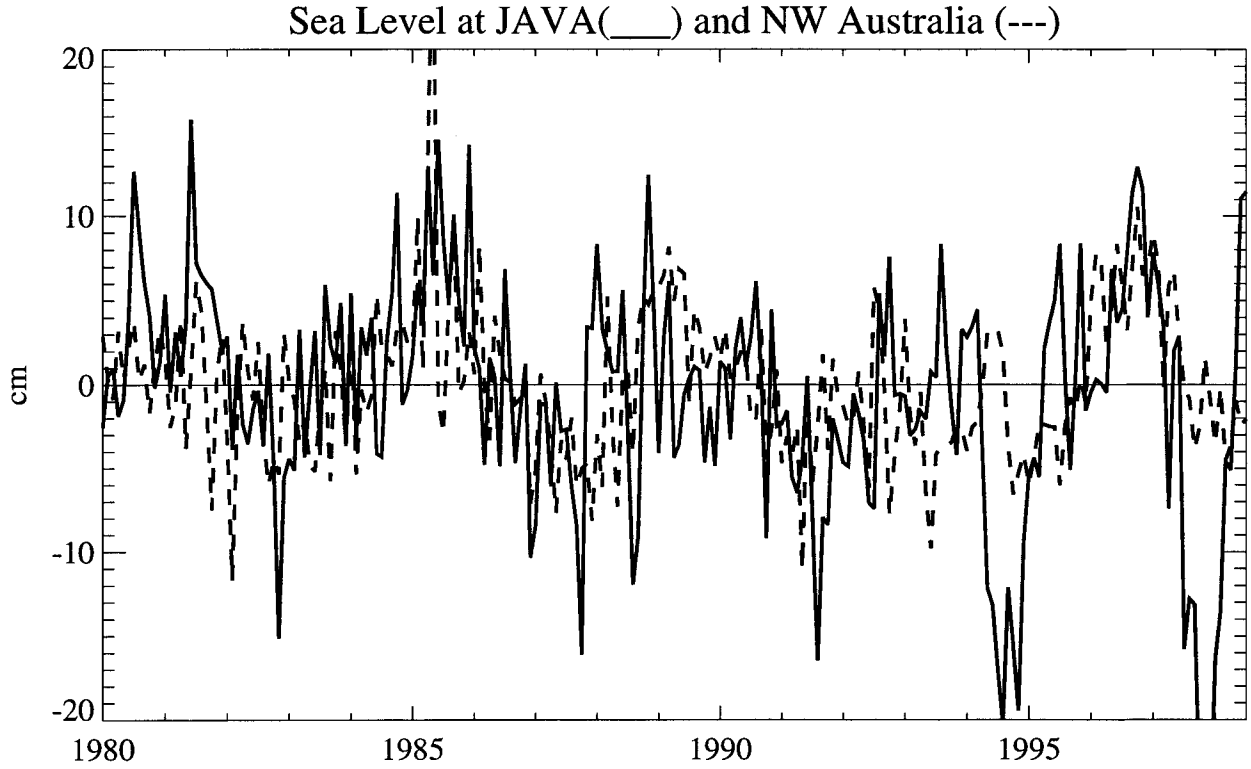
Sea Level at JAVA(___) and NW Australia (---)
cm
20
10
0
-10
-20
1980
1985
1990
1995

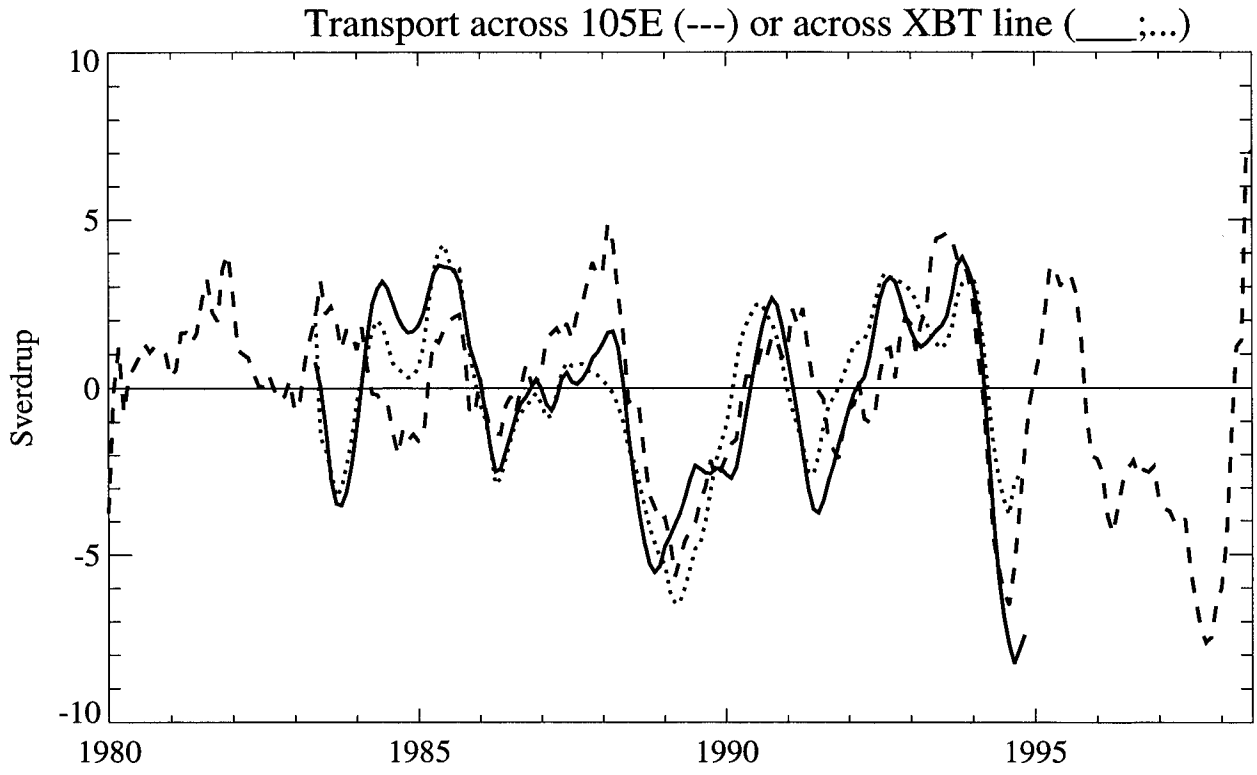
Transport across 105E (---) or across XBT line (___;...)
Sverdrup
10
5
0
-5
-10
1980
1985
1990
1995

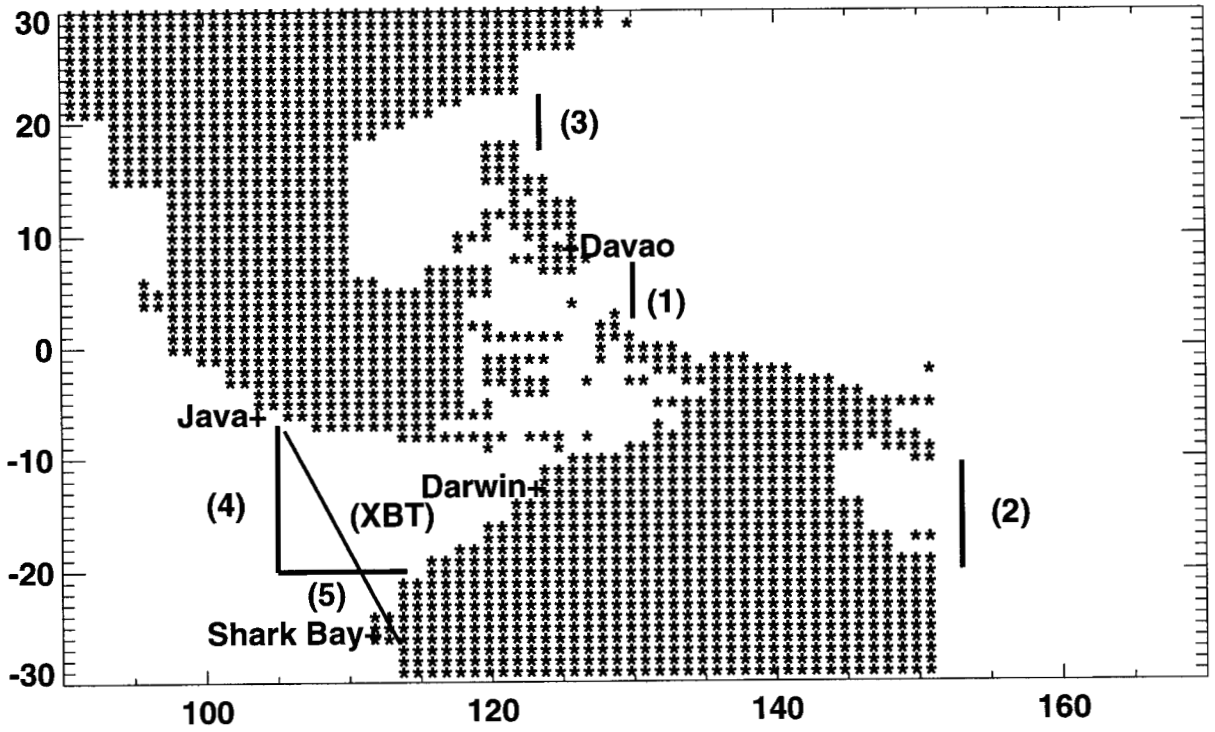
30
20
10
0
-10
-20
-30
100
120
140
160
(3)
Davao
(1)
Java
(4)
(XBT)
Darwin
(2)
(5)
Shark Bay

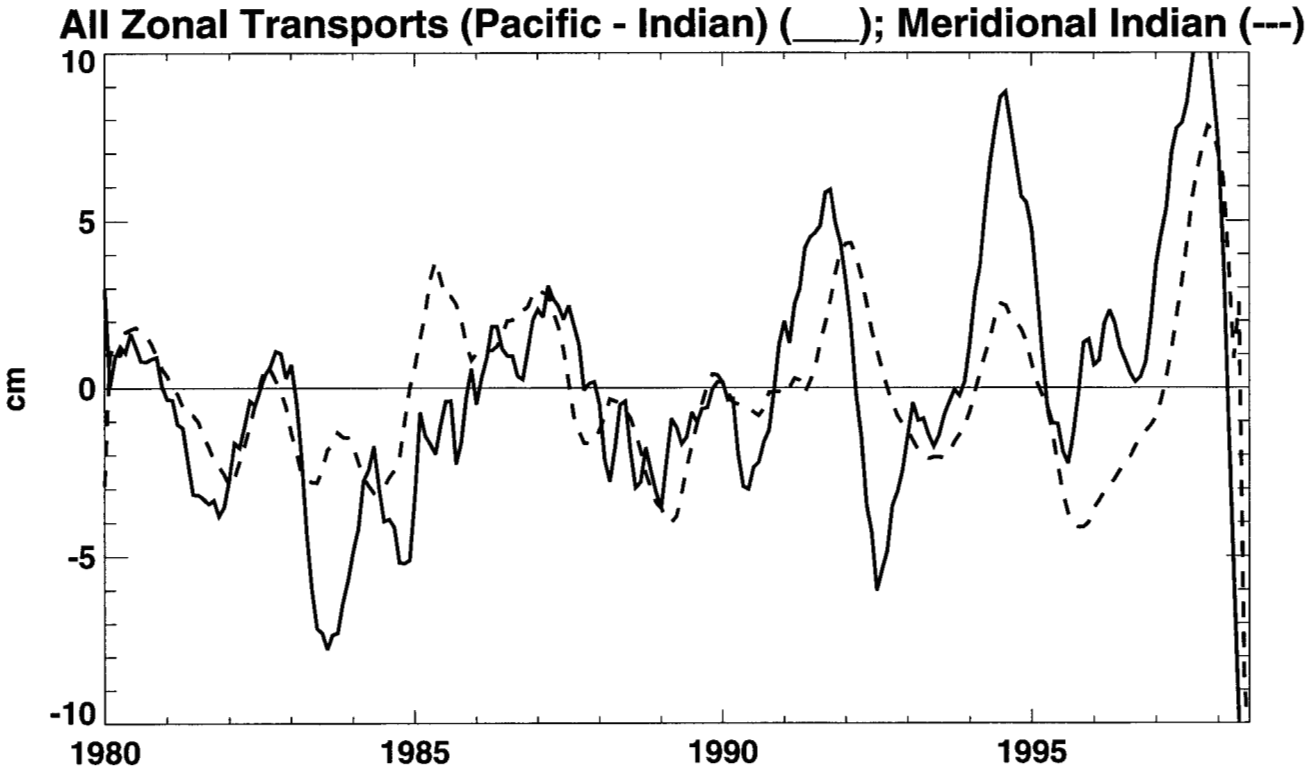
All Zonal Transports (Pacific - Indian) (___); Meridional Indian (---)
10
5
0
-5
-10
cm
1980
1985
1990
1995

SEA LEVEL ANOMALIES (CM) - CONTROL RUN

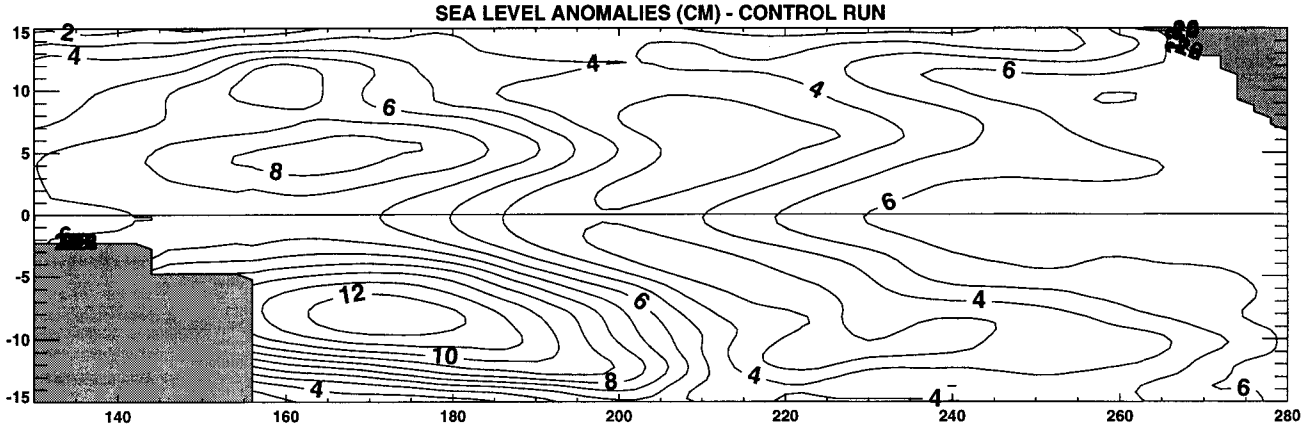

SST ANOMALIES (C) - CONTROL RUN

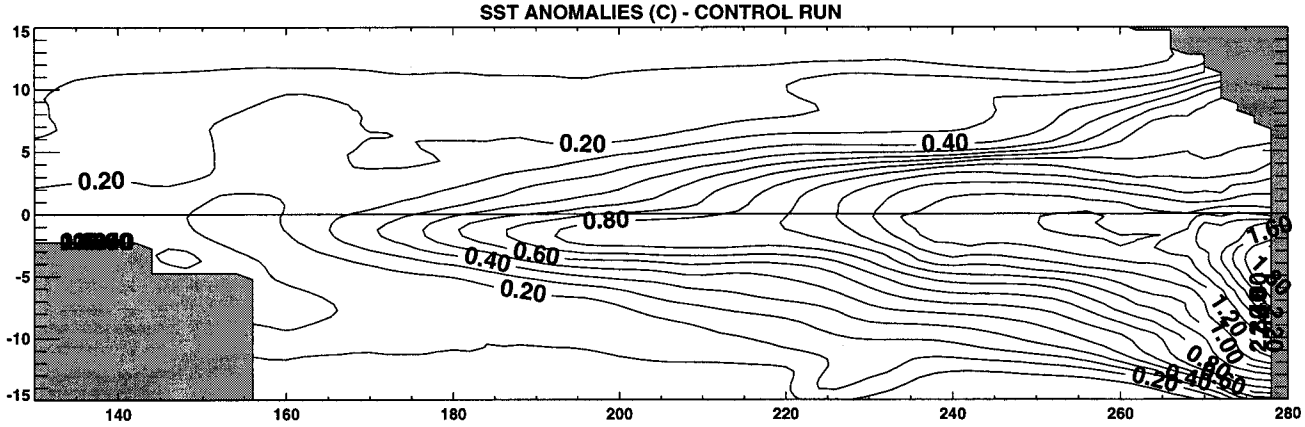

ZONAL WIND STRESS ANOMALIES (DYN/CM2) - CONTROL RUN

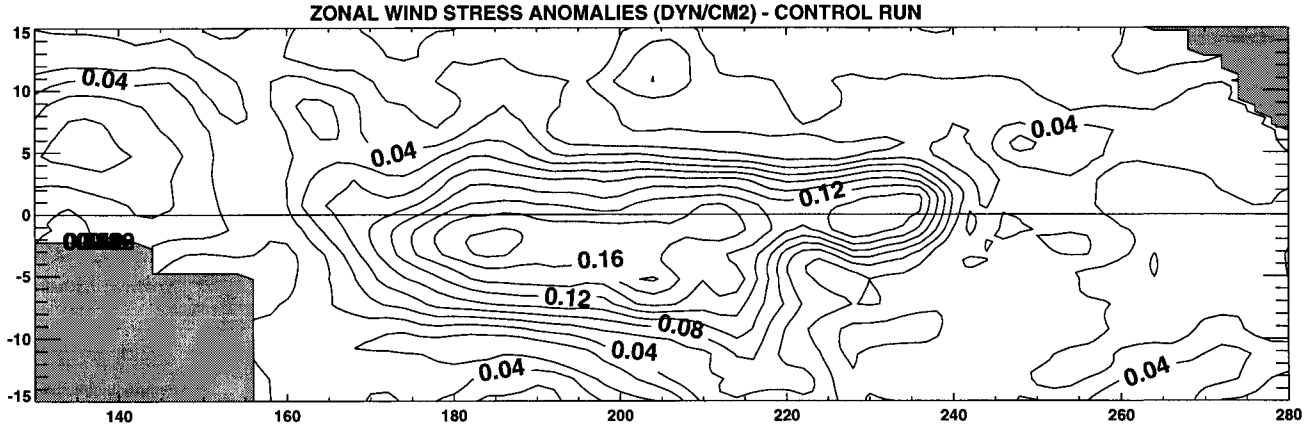

MERIDIONAL WIND STRESS ANOMALIES (DYN/CM2) - CONTROL RUN

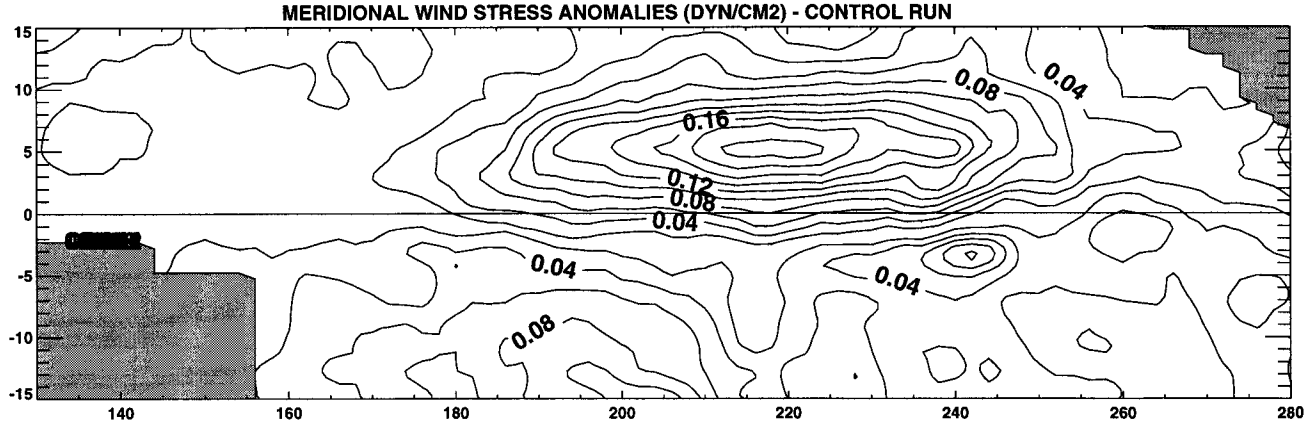

OBSERVED SEA LEVEL ANOMALIES (CM) - Hdyn+TP DATA

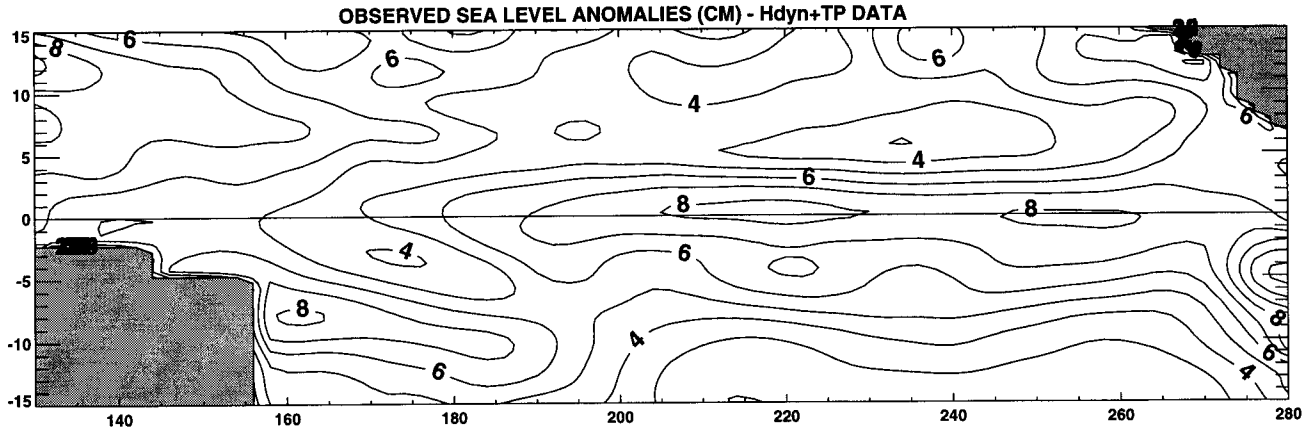

OBSERVED SST ANOMALIES (C) - CAC DATA

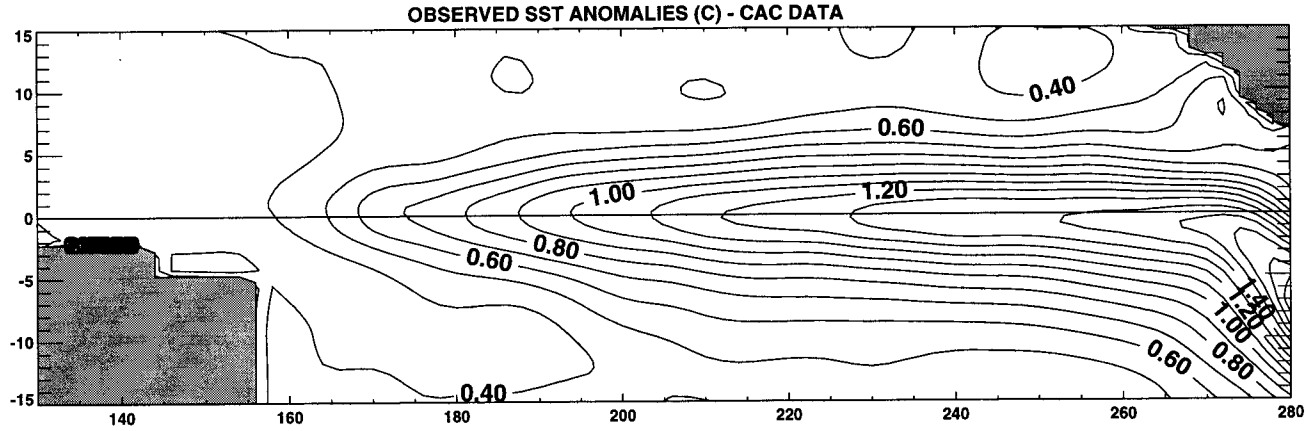

OBSERVED ZONAL WIND STRESS ANOMALIES (DYN/CM2) - Astat.DATA

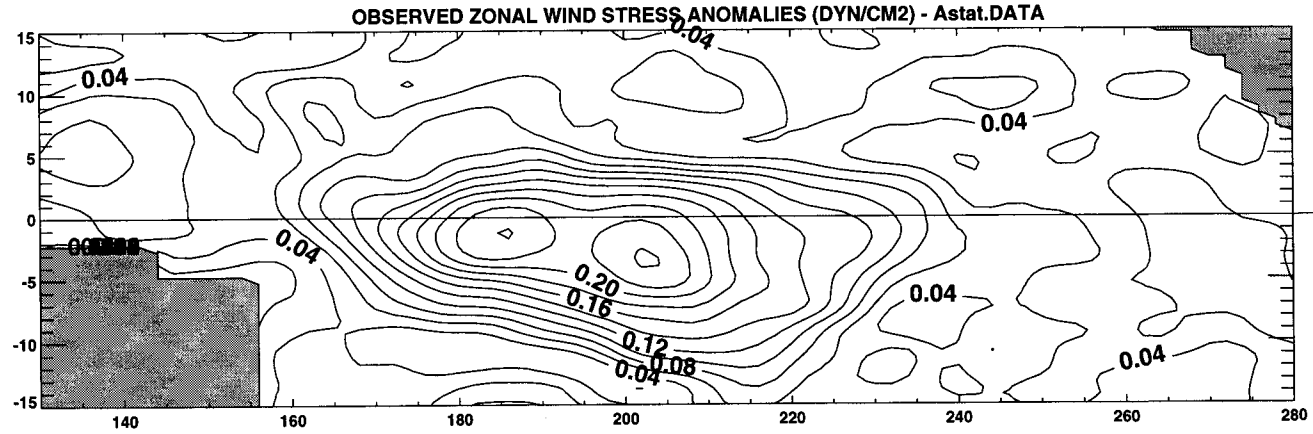

OBSERVED MERIDIONAL WIND STRESS ANOMALIES (DYN/CM2) - Astat.DATA

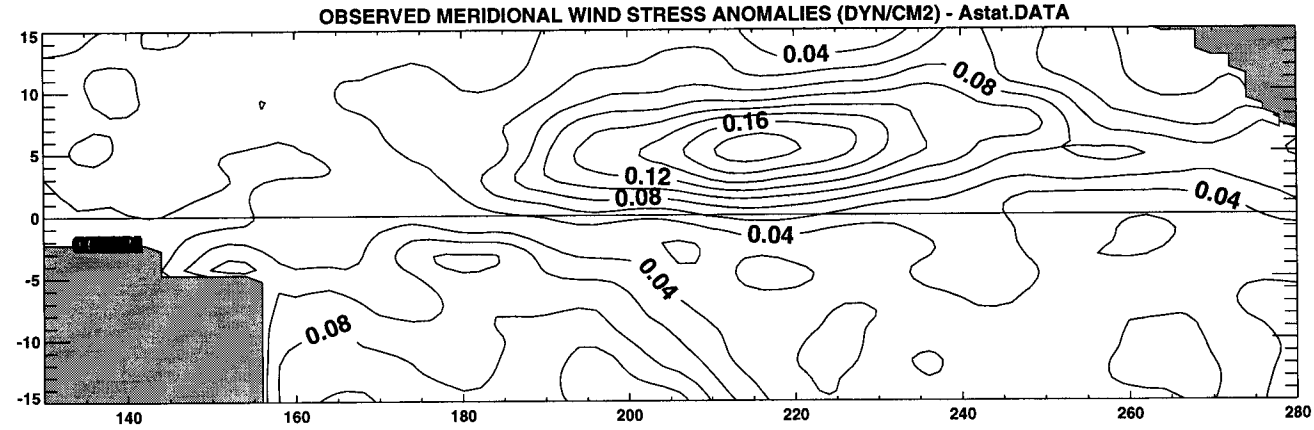

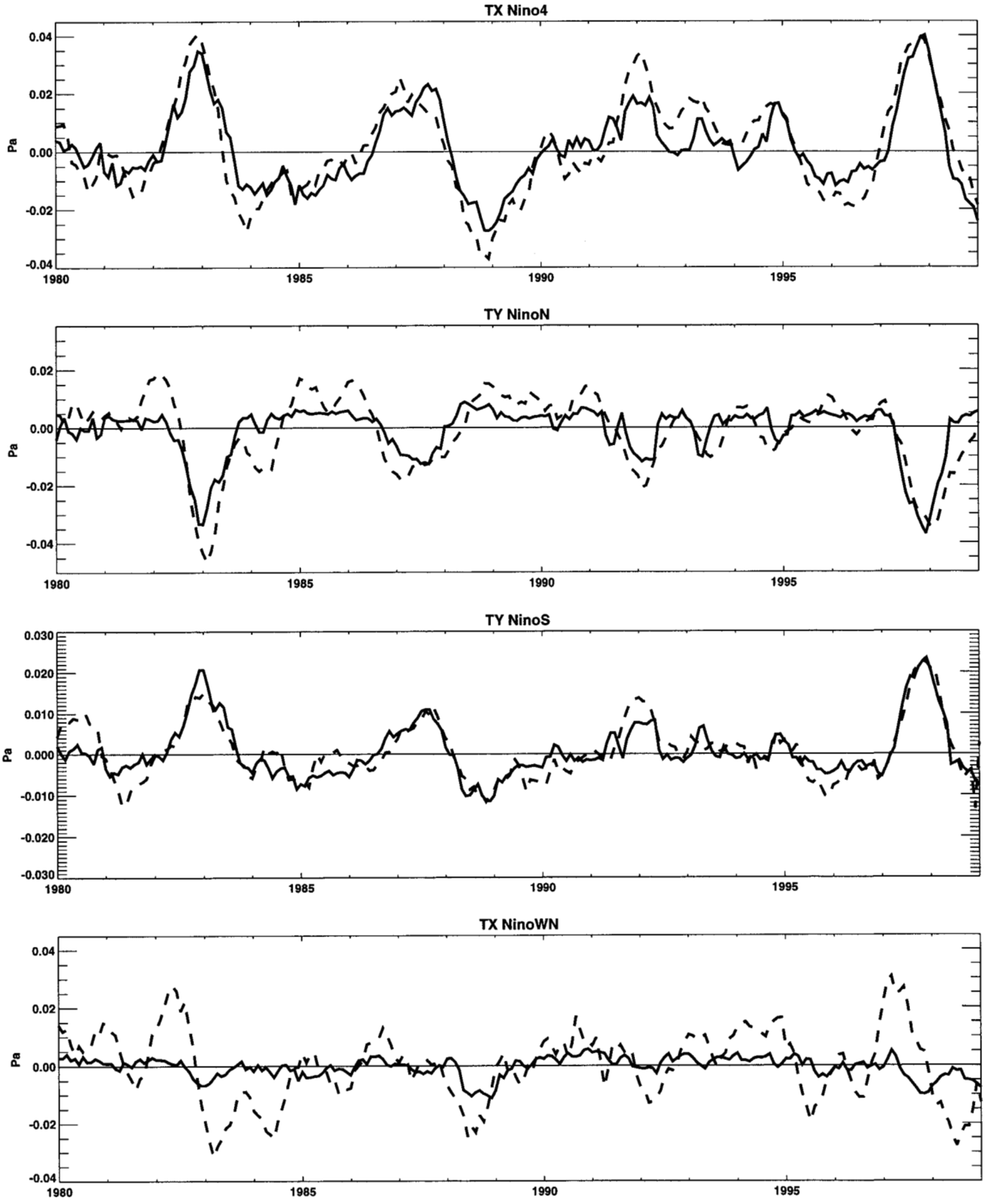
TX Nino4
Pa
0.04
0.02
0.00
-0.02
-0.04
1980
1985
1990
1995
TY NinoN
Pa
0.02
0.00
-0.02
-0.04
1980
1985
1990
1995
TY NinoS
Pa
0.030
0.020
0.010
0.000
-0.010
-0.020
-0.030
1980
1985
1990
1995
TX NinoWN
Pa
0.04
0.02
0.00
-0.02
-0.04
1980
1985
1990
1995

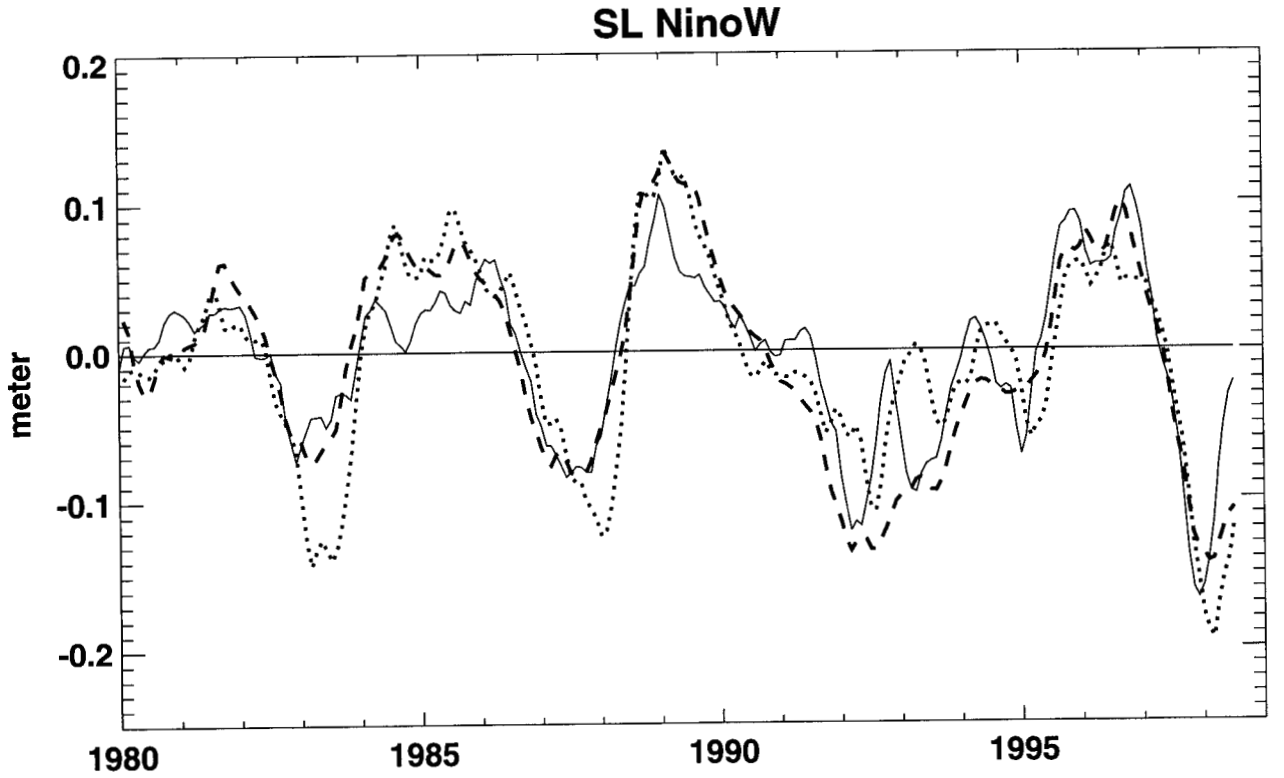
SL NinoW
0.2
0.1
0.0
-0.1
-0.2
meter
1980
1985
1990
1995

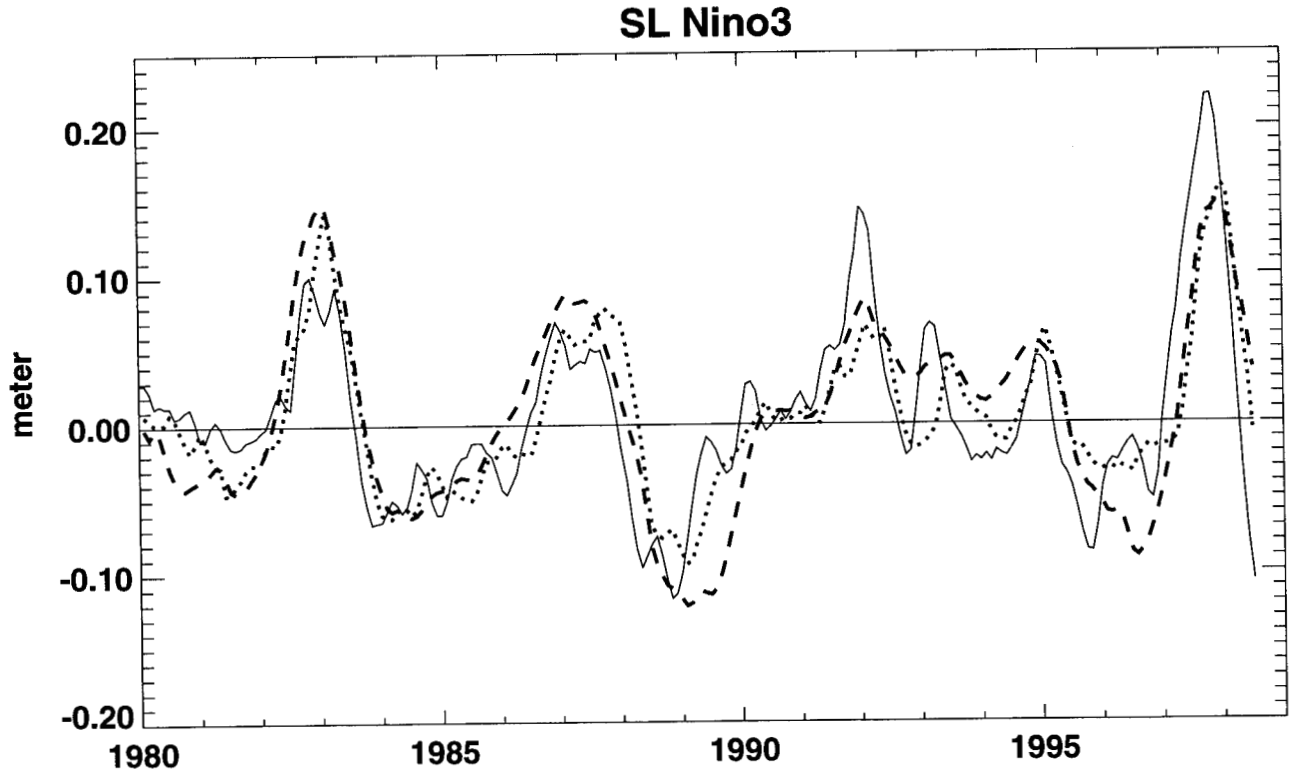
SL Nino3
0.20
0.10
0.00
-0.10
-0.20
meter
1980
1985
1990
1995

1Dab

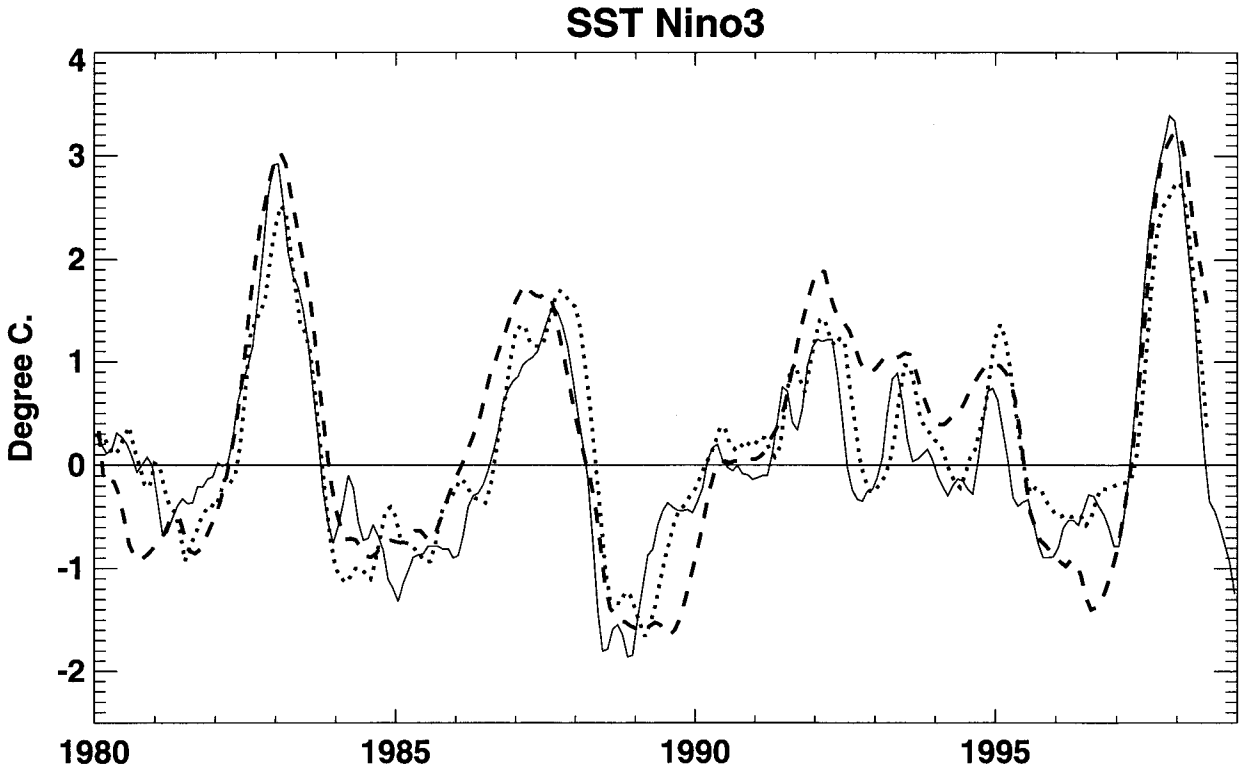
SST Nino3
Degree C.
4
3
2
1
0
-1
-2
1980
1985
1990
1995

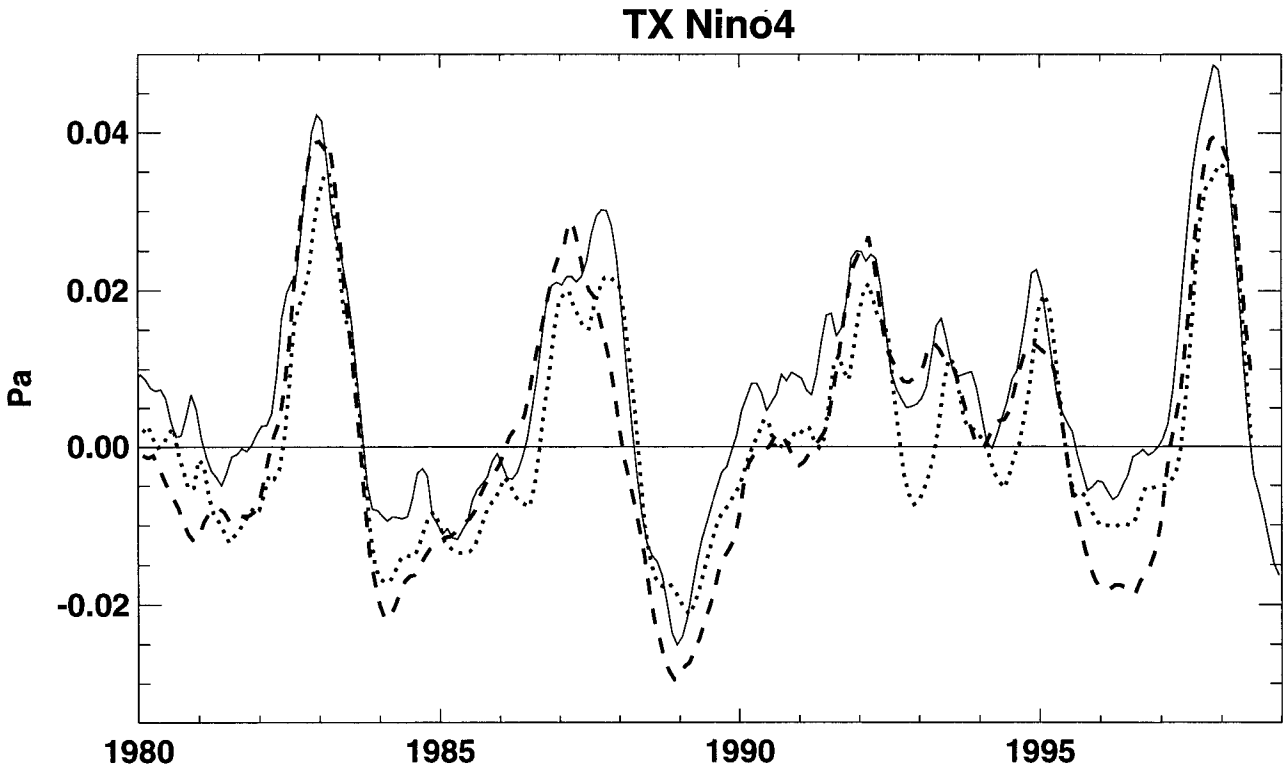
TX Nino4
Pa
0.04
0.02
0.00
-0.02
1980
1985
1990
1995

10od

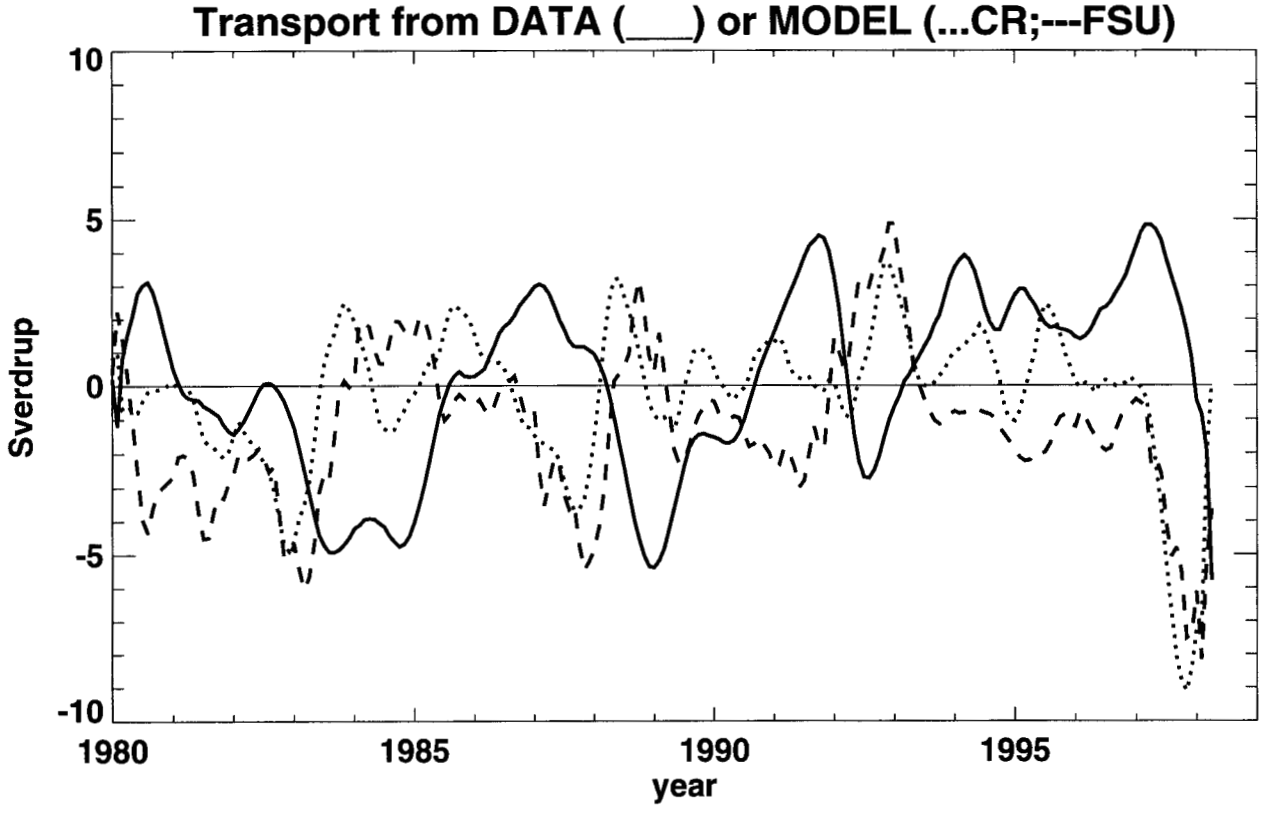
Transport from DATA (___) or MODEL (...CR;---FSU)
Sverdrup
10
5
0
-5
-10
1980
1985
1990
1995
year

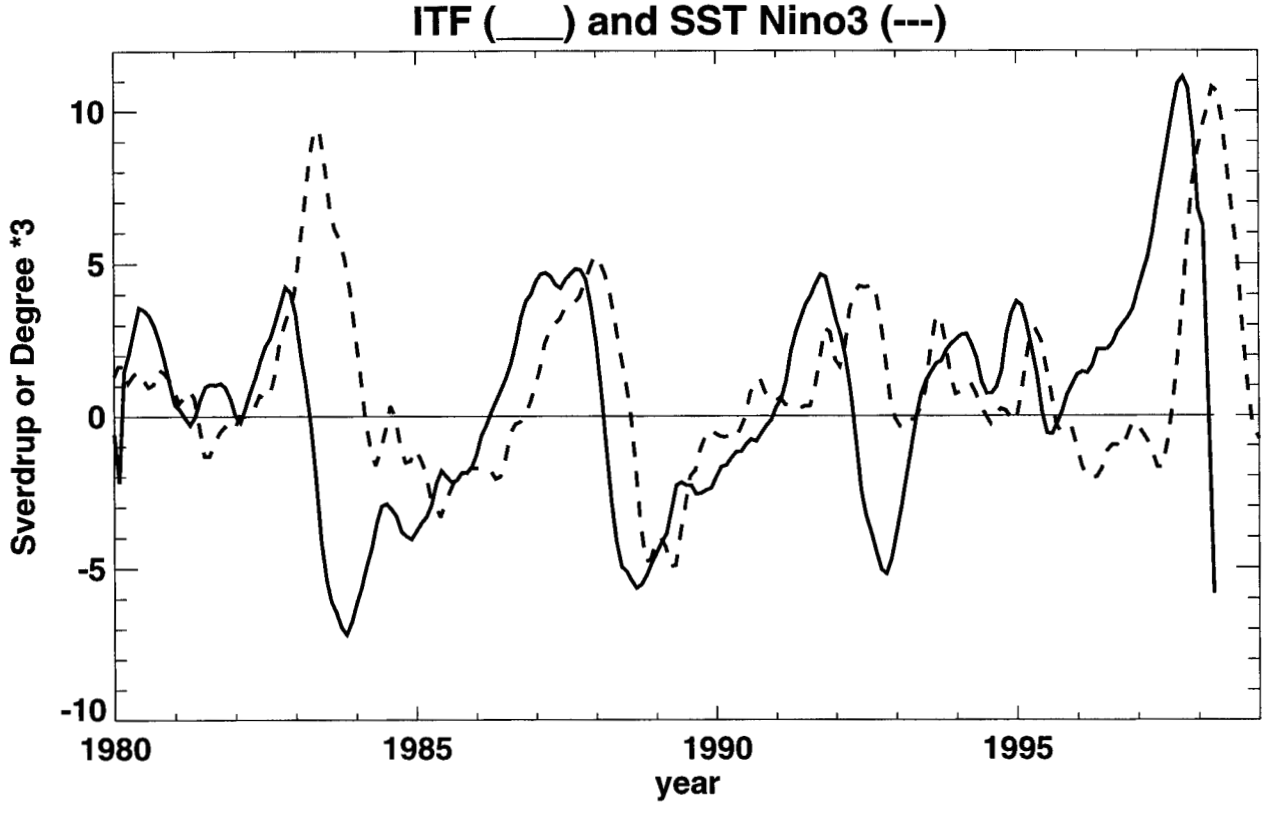
ITF (___) and SST Nino3 (---)
Sverdrup or Degree *3
10
5
0
-5
-10
1980
1985
1990
1995
year

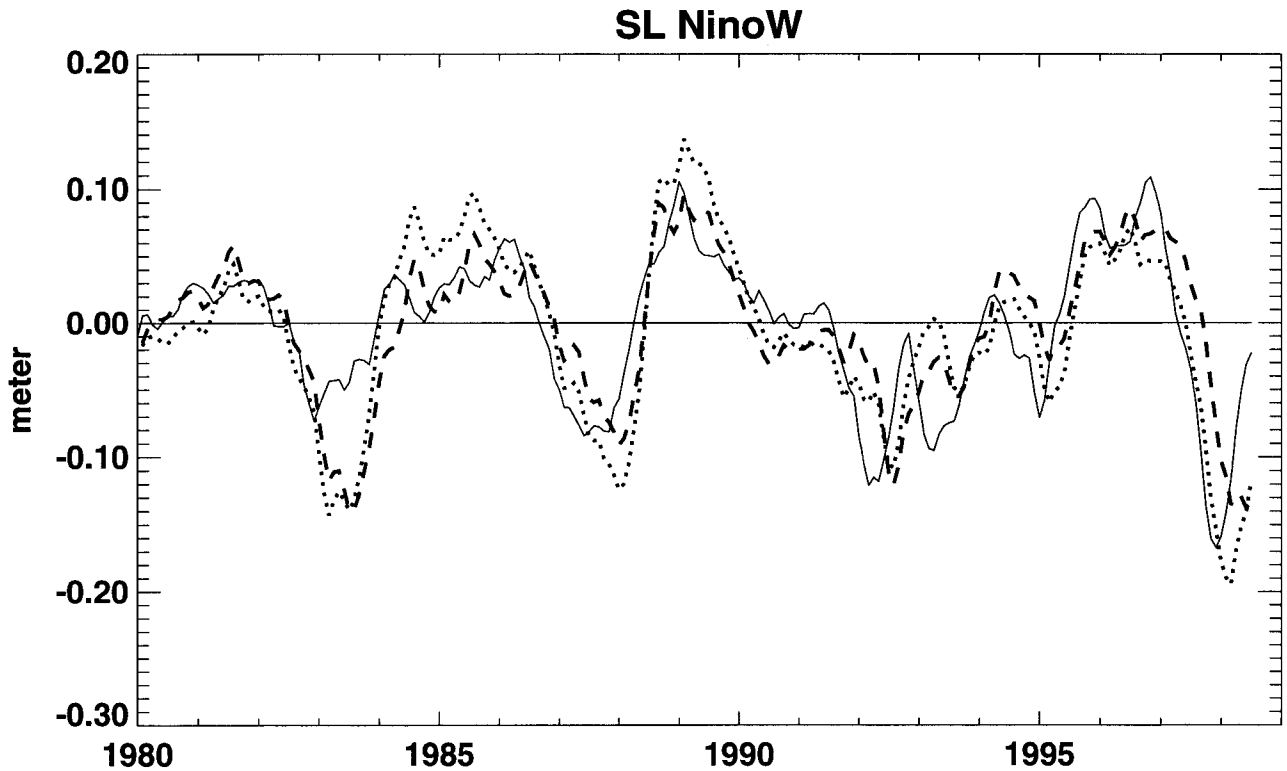
SL NinoW
0.20
0.10
0.00
-0.10
-0.20
-0.30
meter
1980
1985
1990
1995

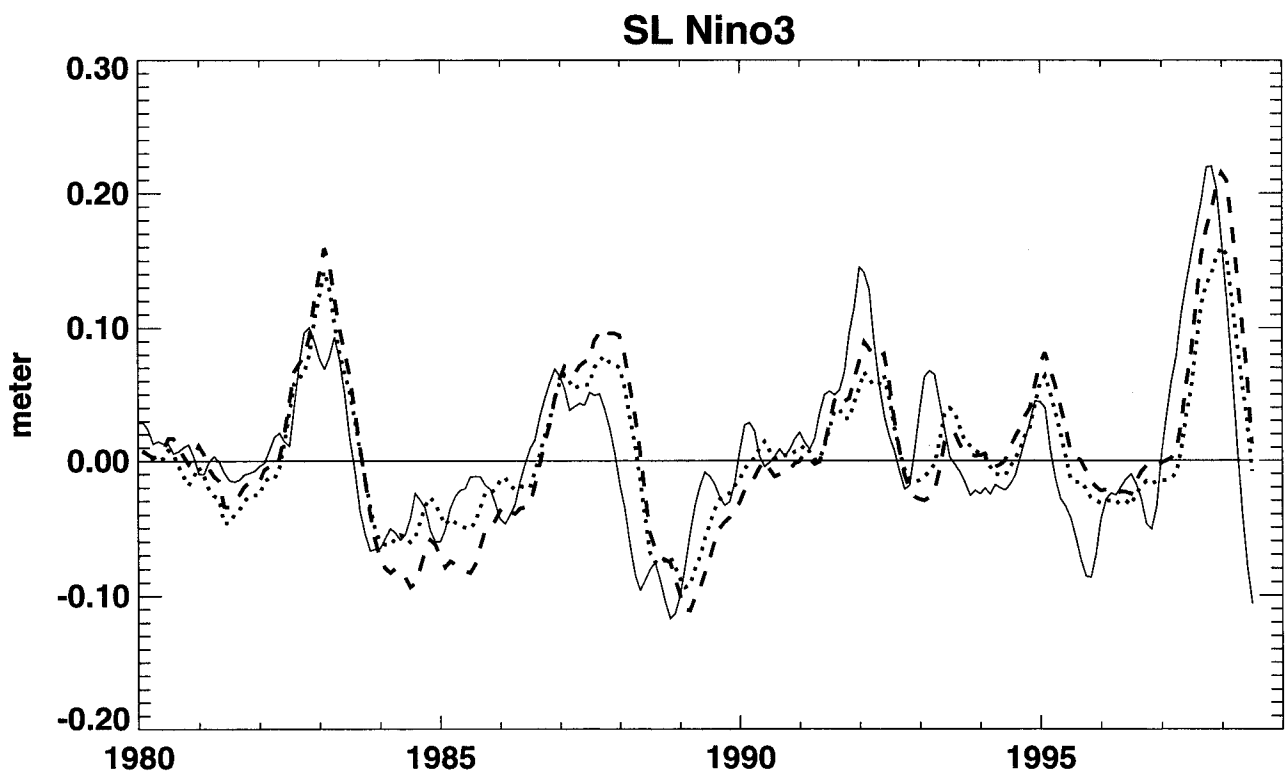
SL Nino3
0.30
0.20
0.10
0.00
-0.10
-0.20
meter
1980
1985
1990
1995

12ab

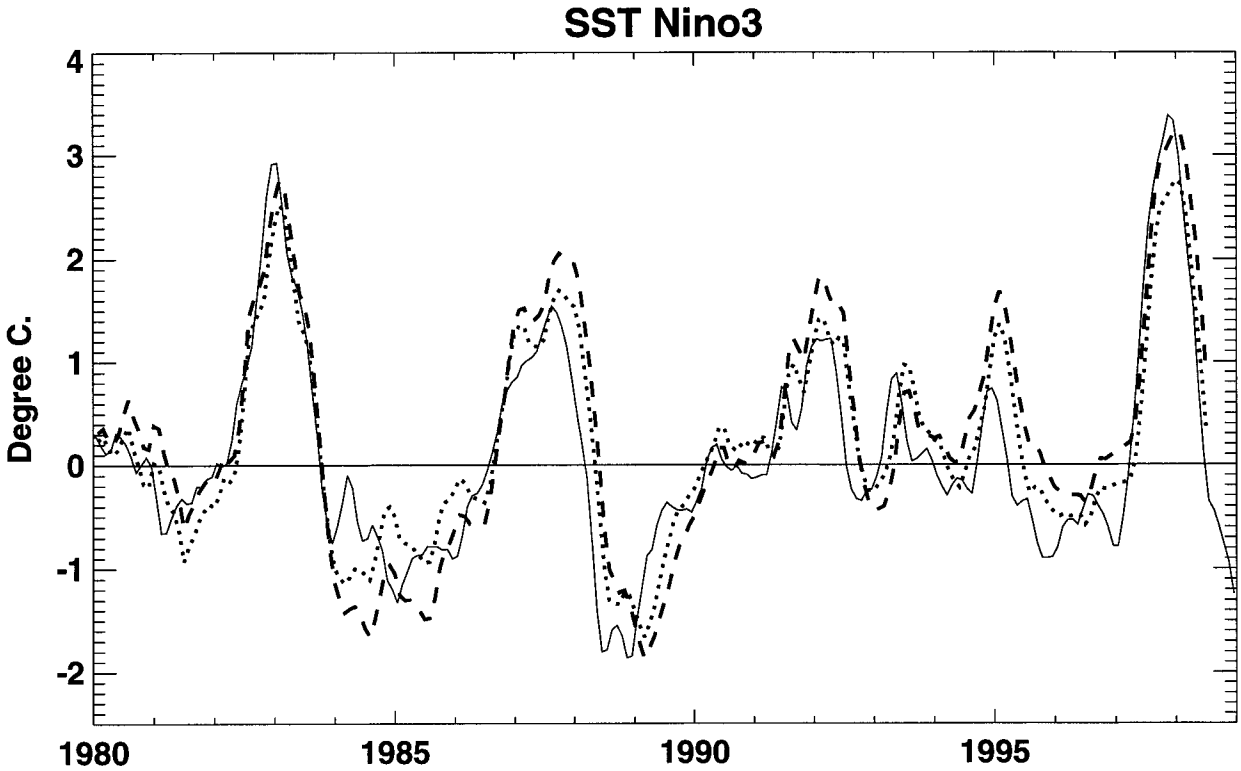
SST Nino3
Degree C.
4
3
2
1
0
-1
-2
1980
1985
1990
1995

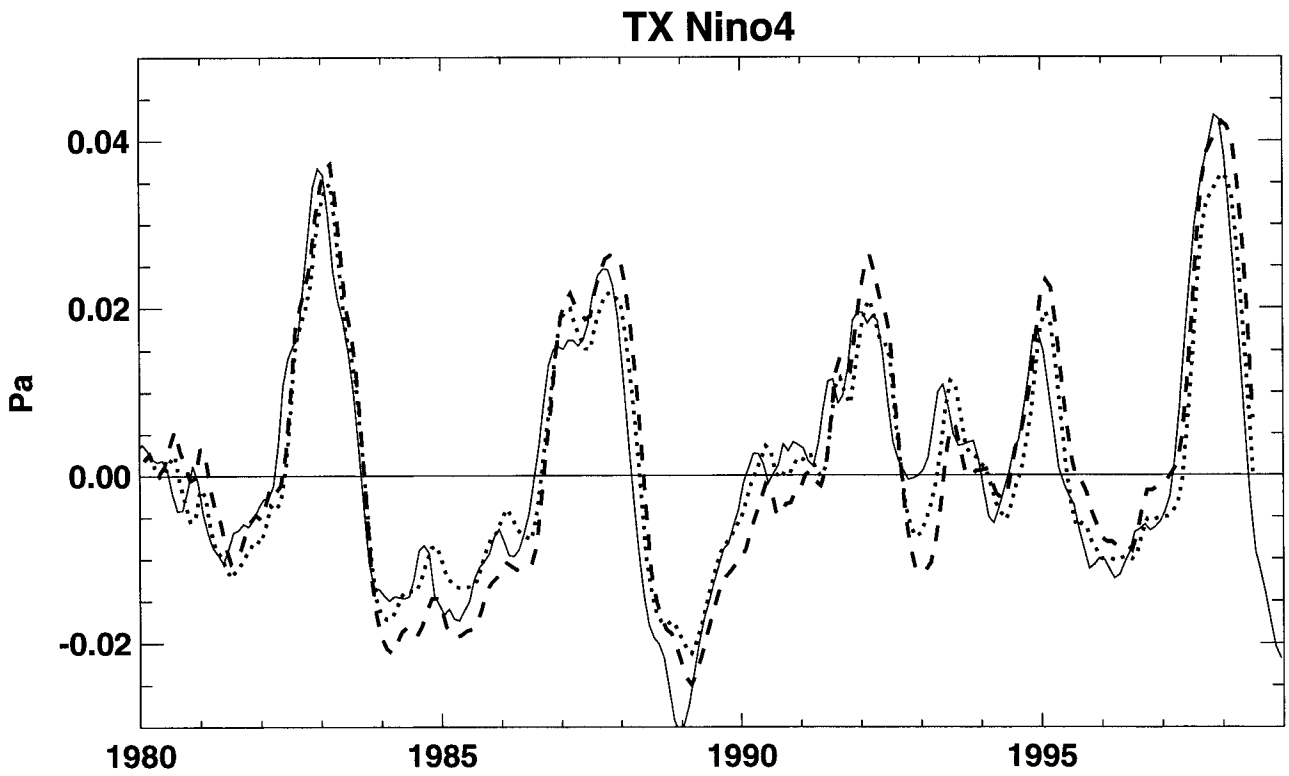
TX Nino4
Pa
0.04
0.02
0.00
-0.02
1980
1985
1990
1995

12cd

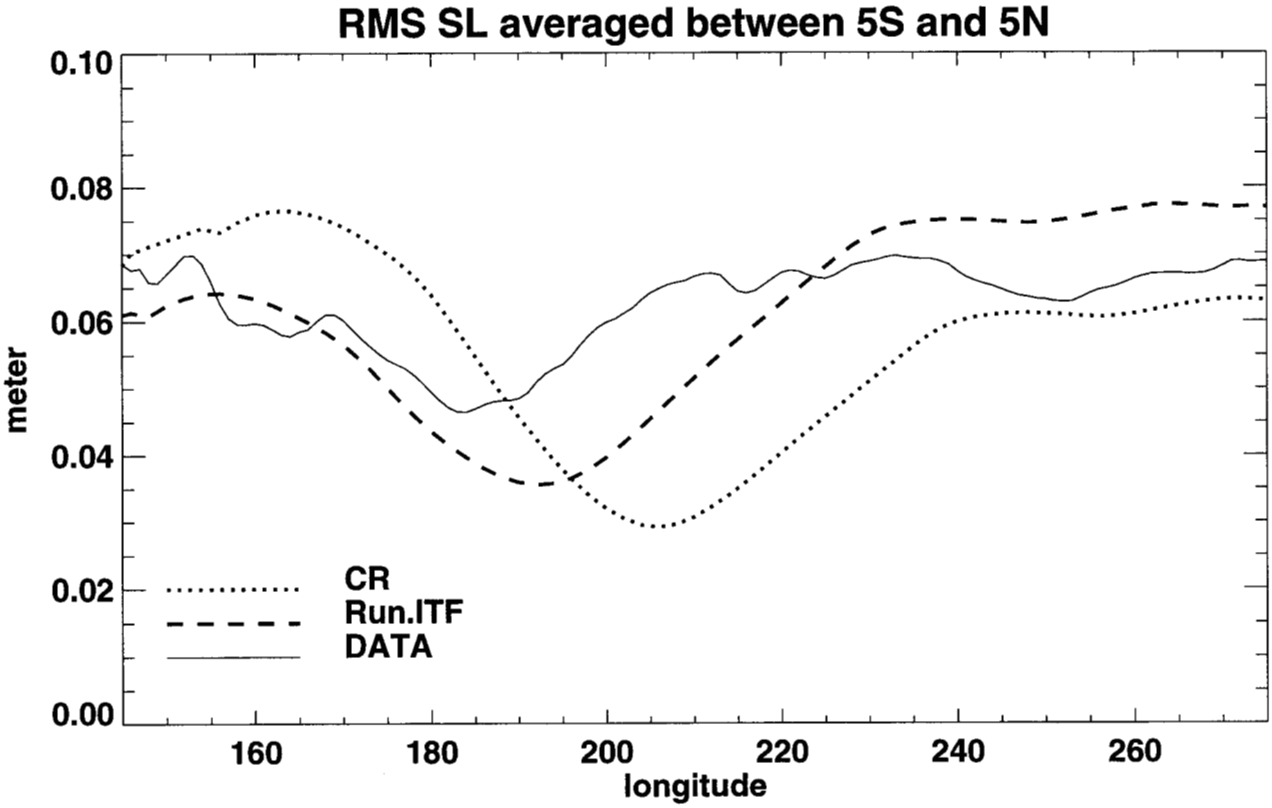
RMS SL averaged between 5S and 5N
0.10
0.08
0.06
0.04
0.02
0.00
meter
CR
Run.ITF
DATA
160
180
200
220
240
260
longitude

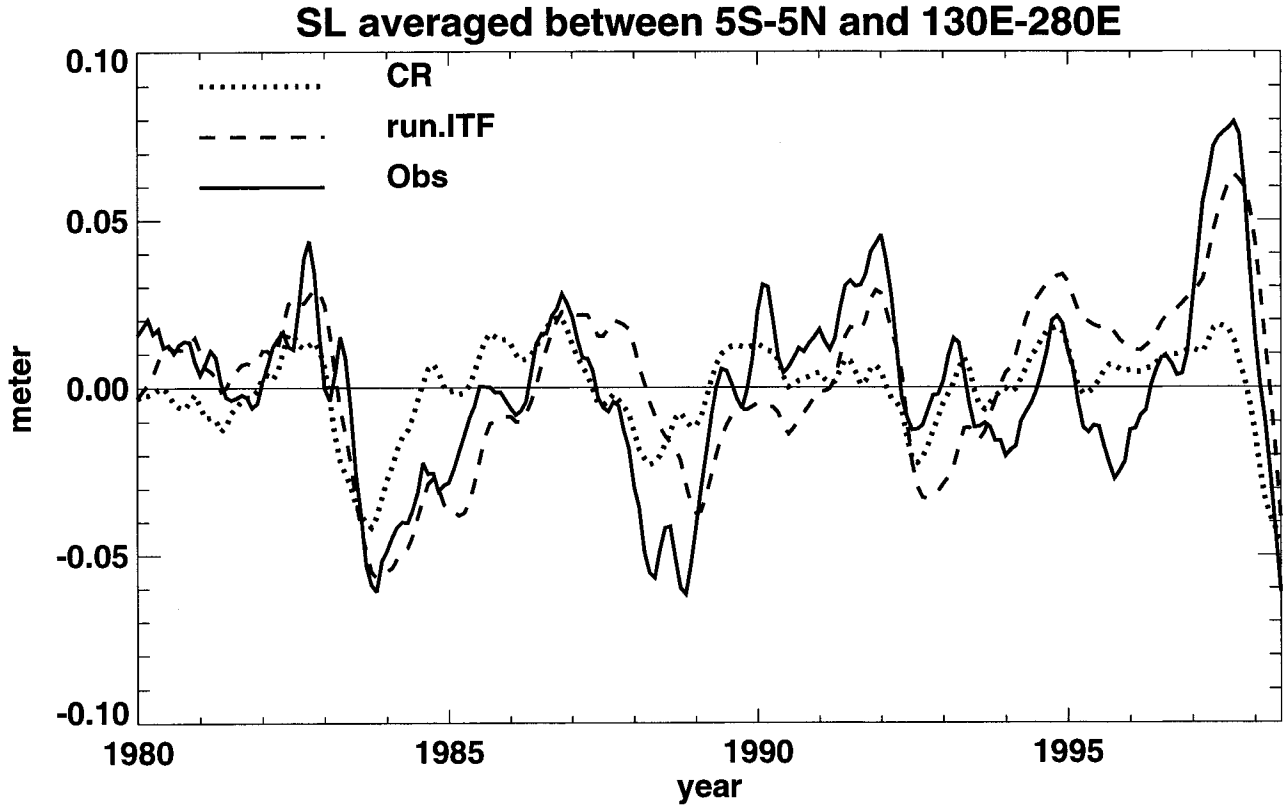
SL averaged between 5S-5N and 130E-280E
CR
run.ITF
Obs
0.10
0.05
0.00
-0.05
-0.10
meter
1980
1985
1990
1995
year

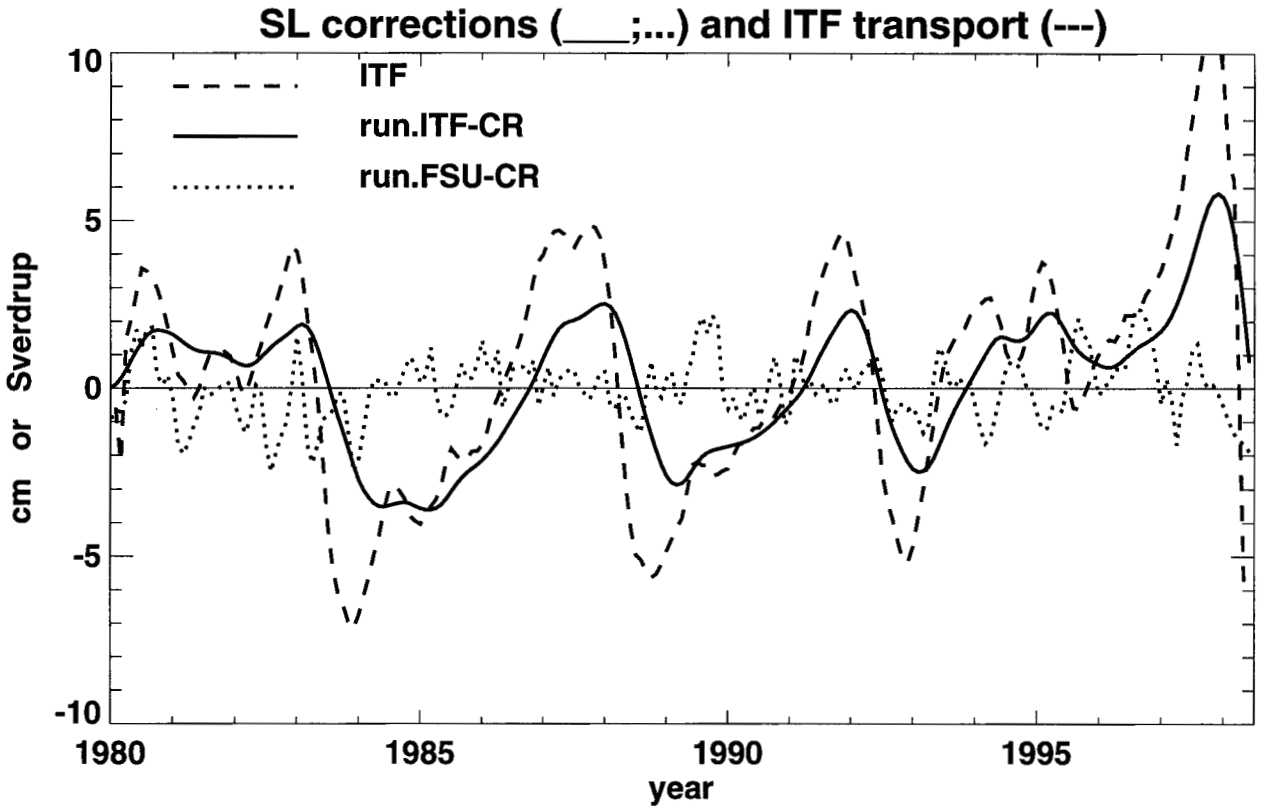
SL corrections (___;...) and ITF transport (---)
ITF
run.ITF-CR
run.FSU-CR
cm or Sverdrup
10
5
0
-5
-10
1980
1985
1990
1995
year

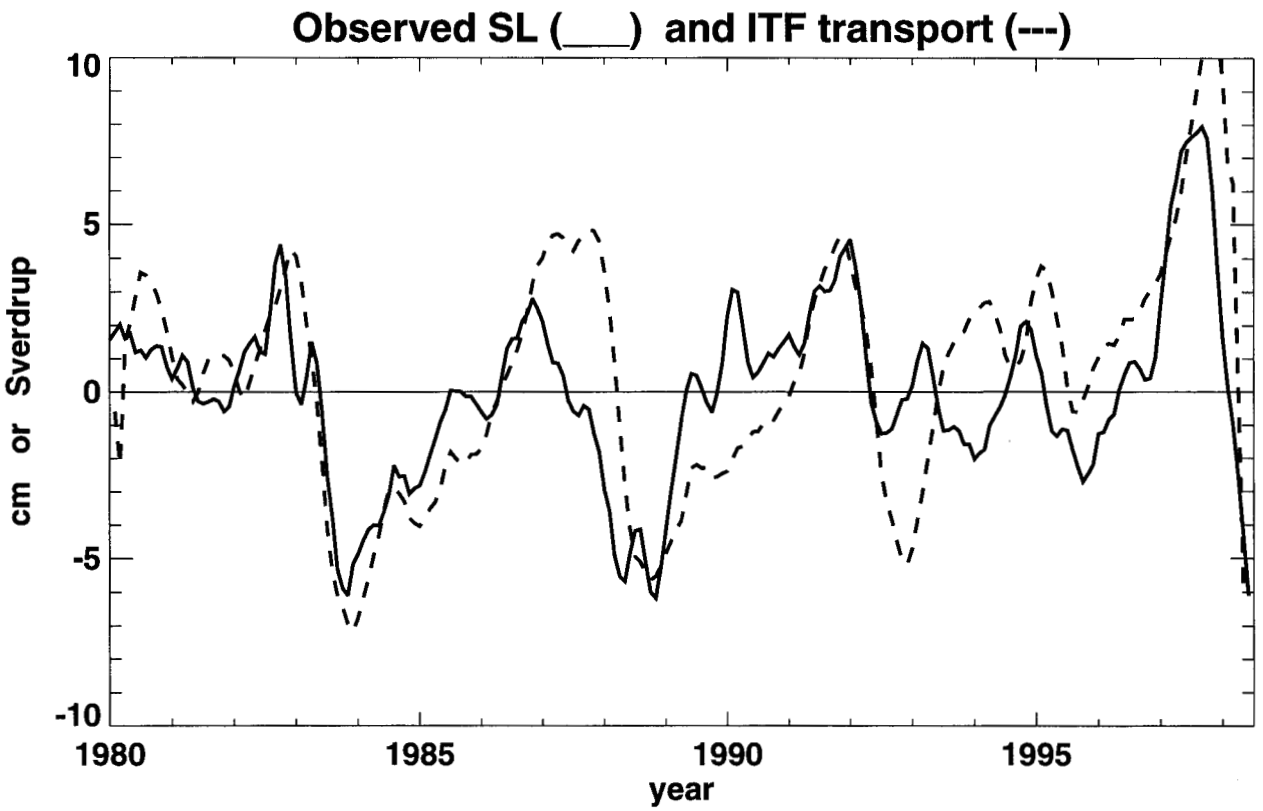
Observed SL (___) and ITF transport (---)
cm or Sverdrup
10
5
0
-5
-10
1980
1985
1990
1995
year

14be

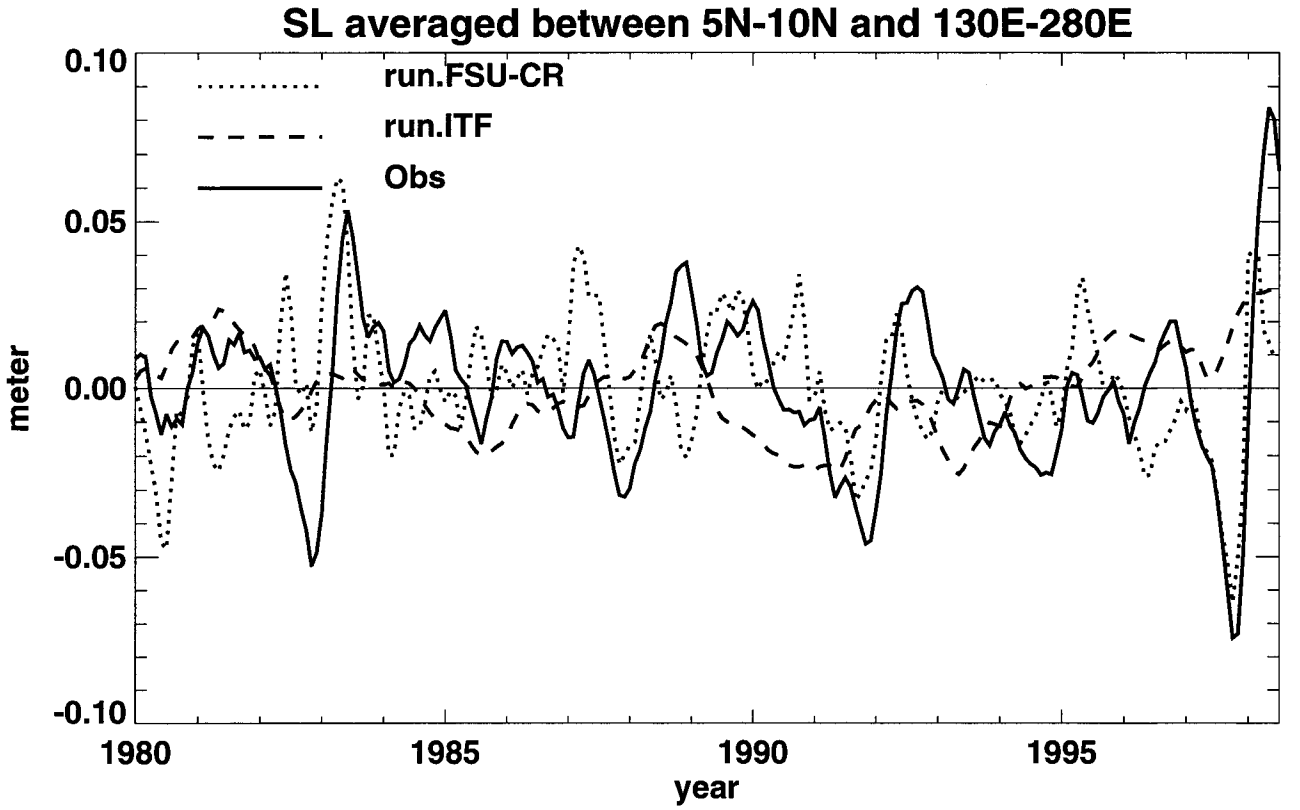
SL averaged between 5N-10N and 130E-280E
run.FSU-CR
run.ITF
Obs
0.10
0.05
0.00
-0.05
-0.10
meter
1980
1985
1990
1995
year

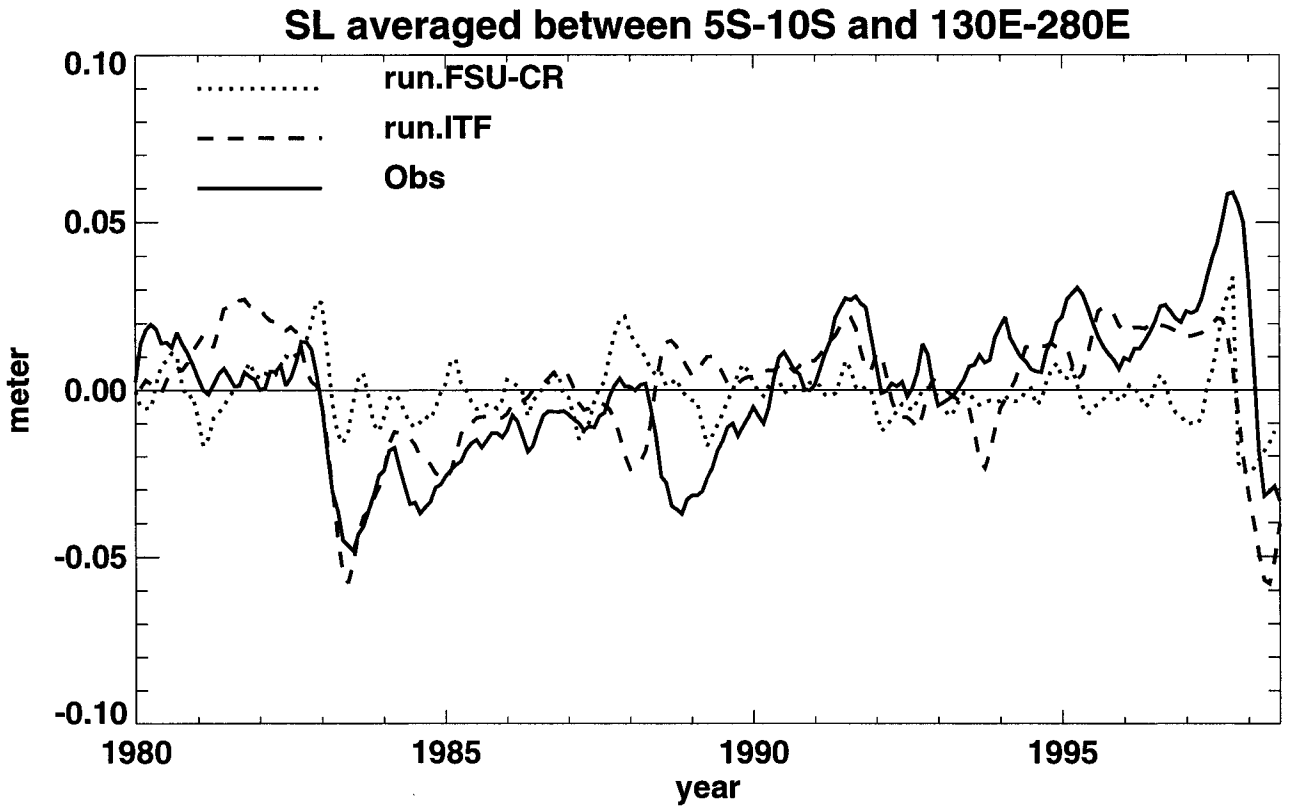
SL averaged between 5S-10S and 130E-280E
run.FSU-CR
run.ITF
Obs
0.10
0.05
0.00
-0.05
-0.10
meter
1980
1985
1990
1995
year